THESIS FOR THE DEGREE OF DOCTOR OF PHILOSOPHY

A Holistic Take on Simulating Battery Electrolytes

FABIAN ÅRÉN

Department of Physics

CHALMERS UNIVERSITY OF TECHNOLOGY

Gothenburg, Sweden 2023

A Holistic Take on Simulating
Battery Electrolytes
FABIAN ÅRÉN
ISBN 978-91-7905-862-3

Doktorsavhandlingar vid Chalmers tekniska högskola
Ny serie nr 5328
ISSN 0346-718X

Department of Physics
Chalmers University of Technology
SE-412 96 Gothenburg
Sweden
Telephone + 46 (0)31-772 1000

Cover:
An AI generated image of a dissected battery filled with a tiny ecosystem of lush greenery in the style of Rembrandt. Generated using DALL·E mini.

Chalmers digitaltryck/Chalmers digital print
Gothenburg, Sweden 2023

A Holistic Take on Simulating Battery Electrolytes
Fabian Årén
Department of Physics
Chalmers University of Technology

Abstract

As powering a sustainable future is a global goal, interest in battery research and technology is at an all-time high. In order to enable a transition to green-tech, many industries, such as the automotive industry, urge for batteries with higher power and energy densities, longer life-times, and that are safer. All these properties are fundamentally limited by the materials employed. Hence humanity's ability to create new energy storage materials need to improve.
The way energy storage materials have been developed up until now have mainly been in the lab. With many other industries benefiting from IT tools the battery industry is seeing a need for new better computational tools to aid in developing new materials. Many put their faith in machine learning algorithms to provide the solution, but those methods are not flawless, and are especially hard to work with when modeling electrolytes. This thesis focuses on physics-based methods to model battery electrolytes, such as DFT, AIMD, and classical MD, and makes a holistic retake on how these methods could be used in unison to better help material developers screen their materials.
Novel electrolyte concepts such as highly concentrated electrolytes and localized highly concentrated electrolytes, both for lithium and calcium batteries, are studied using the aforementioned tools. This thesis also presents how the newly developed CHAMPION software and methods can be used to tie the different methods together and possibly also extend their use by mapping forces on identified interatomic interactions, which may enable much faster turn-around in the simulation protocols.

Keywords: machine learning, multi-scale modeling, electrolytes, DFT, AIMD, MD, lithium-ion batteries

List of Publications

This thesis is based on the following publications in the text they are referred to by their Roman numeral:

I. P.-A. Martin, F. Årén, and P. Johansson, "(Localized) Highly Concentrated Electrolytes for Calcium Batteries," *Batteries & Supercaps*, e202300003, 2023.

II. R. Andersson, F. Årén, A. Franco, and P. Johansson, "Champion: Chalmers hierarchical atomic, molecular, polymeric and ionic analysis toolkit," *Journal of Computational Chemistry*, vol. 42, no. 23, pp. 1632–1642, 2021.

III. R. Andersson, F Årén, A. Franco, and P. Johansson, "Ion transport mechanisms via time-dependent local structure and dynamics in highly concentrated electrolytes," *Journal of the Electrochemical Society*, vol. 167, no. 14, p. 140 537, 2020.

IV. F Årén, R. Andersson, A. Franco, and P. Johansson, "Structure, Dynamics and Ion Transport Mechanisms in Lithium-Ion Battery Electrolytes: Origin and Onset of Highly Concentrated Electrolyte Behavior," Submitted to *Journal of the Electrochemical Society*.

V. F. Årén, R. Andersson, and P. Johansson, "Sidestepping the use of molecular dynamics force fields," In manuscript.

List of Publications not included in this thesis

- C. J. Franko, C.-H. Yim, F Årén, G. Åvall, P. S. Whitfield, P. Johansson, Y. A. Abu-Lebdeh, and G. R. Goward, "Concentration dependent solution structure and transport mechanism in high voltage LiTFSI--Adiponitrile electrolytes," *Journal of The Electrochemical Society*, vol. 167, no. 16, p. 160 532, 2020.

- T. Lombardo, M. Duquesnoy, H. El-Bouysidy, F Årén, A. Gallo-Bueno, P. B. Jørgensen, A. Bhowmik, A. Demortière, E. Ayerbe, F. Alcaide, M. Reynaud, J. Carrasco, A. Grimaud, C. Zhang, T. Vegge, P. Johansson, and A. A. Franco, "Artificial intelligence applied to battery research: Hype or reality?" *Chemical Reviews*, vol. 122, no. 12, pp. 10 899–10 969, 2022.

- P. Johansson, S. Alvi, P. Ghorbanzade, M. Karlsmo, L. Loaiza, V. Thangavel, K. Westman, and F Årén, "Ten ways to fool the masses when presenting battery research," *Batteries & Supercaps*, vol. 4, no. 12, pp. 1785–1788, 2021.

Contribution Report

I. I planned the computational part of this study together with PAM. I performed the DFT calculations and contributed to the Raman analysis comparing computational and experimental data. I wrote the computational parts of the paper.

II. I aided RA in developing the method and contributed in implementing it in code. I performed all the AIMD simulations. I co-authored parts of the paper.

III. I performed the AIMD simulations and I assisted in the CHAMPION analysis. I co-authored parts of the paper.

IV. I performed a majority of the AIMD simulations and analysed the results using CHAMPION. I wrote the final draft of the paper.

V. I was the main author of the paper. I developed the method based on ideas developed together with RA and I designed the study. I implemented the methods in code and I performed all the simulations and analysis.

Table of Contents

List of Tables and Figures

List of Abbreviations

ACN	Acetonitrile
AIMD	*ab initio* Molecular Dynamics
AM	Active Material
BOMD	Born-Oppenheimer Molecular Dynamics
CaB	Calcium Battery
CEI	Cathode Electrolyte Interphase
CN	Coordination Number
CPMD	Carr-Parrinello Molecular Dynamics
DFT	Density Functional Theory
DFTB	Density Functional Tight Binding
DMC	Dimethyl Carbonate
DOD	Depth of Discharge
DOE	Design of Experiment
DSD	Dynamic Structure Discovery
EA	Evolutionary Algorithm
EC	Ethylene Carbonate
ESW	Electrochemical Stability Window
FF	Force Field
GP	Gaussian Process
GPW	Gaussian Plane Wave
GA	Genetic Algorithm
HCE	Highly Concentrated Electrolyte
HOMO	Highest Occupied Molecular Orbital
KPI	Key Performance Indicator
LCO	$LiCoO_2$
LE	Liquid Electrolyte
LJ	Lennard Jones
LHCE	Localized Highly Concentrated Electrolyte
LIB	Lithium-Ion Battery
LiTFSI	Lithium bis(trifluoromethanesulfonyl)imide
LP30	1 M $LiPF_6$ in EC/DMC
LUMO	Lowest Unoccupied Molecular Orbital
MD	Molecular Dynamics
ML	Machine Learning
NMR	Nuclear Magnetic Resonance
NN	Neural Network
pRDF	partial Radial Distribution Function

RQK	Rational Quadratic Kernel
RMSE	Root Mean Squared Error
SAXS	Small Angle X-ray Scattering
SCF	Self-Consistent Field
SEI	Solid Electrolyte Interphase
SF	Symmetry Function
SHE	Standard Hydrogen Electrode
SN	Solvation Number
SOAP	Smooth Overlap of Atomic Position
SOC	State of Charge
xTB	Extended Tight Binding

1
Introduction

The source of everything separating someone born in the 21st Century and someone born during the neolithic era has been argued to be the technology available to them [1]. Whether or not this is true is not a discussion for this thesis, however, at the basis of technological advancement is advancement in materials science. Hence the study of materials science is fundamental to making all technological innovation possible. The idea that technology is merely an extension of human capabilities has been prevalent since the late 19th, early 20th Century with thinkers such as Ralph Waldo Emerson [2] and Henry Ward Beecher [3] popularising the idea with quotes such as *"All the tools and engines on earth are only extensions of man's limbs and senses" - Emerson* and *"A tool is but the extension of a man's hand and a machine is but a complex tool." - Beecher.*

Hence, if we want to advance as a society we must at some point first advance the technology at our disposal, which starts with the materials we can make use of. The mid 20th and early 21st Centuries have been filled with advances in materials science and humanity's understanding of the world around us has leapt forward unprecedentedly. This development culminated with the period between $\sim$ 1970 and 2020 which have been dominated by an exponential development in semi-conductor materials. This exponential development pattern was made famous by the founder of Intel, Gordon E. Moore in 1965, and is commonly referred to as Moore's law. The adherence of semi-conductor materials to Moore's law has set the expectation for all materials development to follow this trend.

Materials science in general however cannot be expected to follow the same speed, which is exemplified in *e.g.* the energy storage materials field. With the increased need for clean energy one of the most important research fields is the development of energy storage materials, such as materials for batteries [4]. Currently the state-of-the-art battery technology, the lithium-ion battery (LIB) has come a long way since its introduction in the 1990's by Sony [5]. Having an energy density of 200 Wh/l or 80 Wh/kg enabled the widespread adoption of handheld electronics. Today the energy densities have more than tripled, which is an excellent development, but nowhere near an exponential increase. To address this and try to improve the development speed of materials one must first address one of the major problems of material research which is the trial and error process used to discover new materials, popular both within academia and industry. Looking at other fields [6], [7], it is clear that computational approaches have a great potential to be an alternative solution making the process more effective. However, even though it is possible to exactly

solve any system in theory, in the words of *Paul Dirac* [8]:

"The underlying physical laws necessary for the mathematical theory of a large part of physics and the whole of chemistry are thus completely known, and the difficulty is only that the exact application of these laws leads to equations much too complicated to be soluble.",

material simulations at the molecular level are difficult, even if far from practically impossible to perform. One of the most effective techniques to simulate systems at the molecular scale is density functional theory (DFT) [9]. Being able to simulate molecules accurately to achieve understanding quickly breaks down as the system size increases due to DFT lacking the ability to simulate dynamics, which becomes more important for explaining properties emerging at larger system sizes. Hence an additional tool in our computational tool box is needed; one able to simulate dynamics of systems of any composition at a mesoscopic scale with quantum accuracy. In this thesis DFT is used in Paper **I** to identify the origins of spectroscopic observations and showcase the value of simulation to explain experimental data determined by static properties.

Studying systems larger than a few molecules, however, requires a different tool. Molecular dynamics (MD) simulations have been a functional tool since the 1950's [10], [11] and the method was the grounds for the 2013 Nobel Prize in Chemistry [12]. However, even though MD simulations have been shown numerous times to aid materials scientists in their work [13]–[15], the method has several drawbacks. One of the most significant challenges is the methods used to evaluate inter-particular forces, which is where two distinct methods, *ab initio* MD (AIMD) and classical MD (simply referred to as MD), mainly differ. Paper **II**, **III**, and **IV** display a proof-of-concept for our patented method of analysing MD trajectories. Specifically, AIMD is used to propagate the systems, generating realistic structures, showcasing the power of AIMD for understanding battery materials in particular cases, and in general displaying the potential of MD for studying batteries.

In order to enable MD simulations of non-conventional electrolytes at nano-scale, a system for generating accurate force fields (FF's) has to be developed, with the development of a universal FF being the holy grail. Many attempts have been made and in general these attempts have been quite successful, using different machine learning (ML) approaches, mainly neural networks (NN) of different types [16]–[18]. Even though ML techniques have many advantages there are certain drawbacks, such as the large data-sets needed and the long times needed for training, as well as the lack of an understanding of the underlying physical phenomenon causing the predicted behaviour, colloquially called a "black box" [19]. In paper **V** a method to easily generate accurate FFs on the go for specific systems is presented, based upon a generalisation of the methods developed by Åvall and Johansson to extract effective pair-wise forces and interaction energies from AIMD [20] combined with the method for structural detection developed in papers **II** - **IV**. These generalised FFs makes away with most of the problems of ML methods presented above and

can be used as a stepping stone towards universal FFs.

This thesis show how simulation methods at multiple scales can be used to model electrolytes and effectively predict important material properties, but foremost it finally proposes a novel method to generate FFs with low computational cost and DFT accuracy. All in order to help streamline the development of materials in a rapidly changing landscape of modern battery electrolytes. Being able to obtain properties such as transport numbers, partial conductivity, partial electrical mobility *etc.* accurately through computations open up a whole new world of screenings and smarter approaches to materials development.

2

Methods for Molecular Level Modelling of Battery Electrolytes

This thesis aims to holistically look at how battery electrolytes are modelled today, and propose a novel way to set up simulations from bulk, all the way down to local DFT structure calculations (Fig 2.1). Simulations are capable of predicting several properties of interest when designing battery electrolytes, such as: ionic conductivity, diffusivity, electrochemical stability, thermal stability, just to name a few, which should make them important tools in every battery engineers arsenal. Having such a split focus on the use of computational methods at multiple scales, a natural start is with a description of the methods in isolation, which will be provided in this section. However, for electrolytes it is important to also study the interconnectivity between the physics ranging from molecules and up. This concept is called multi-scale modelling, a field of science dedicated to studying and solving problems which have important features at multiple temporal and spatial scales [21]. In paper **V** an attempt is made to marry the different scales and will be discussed further.

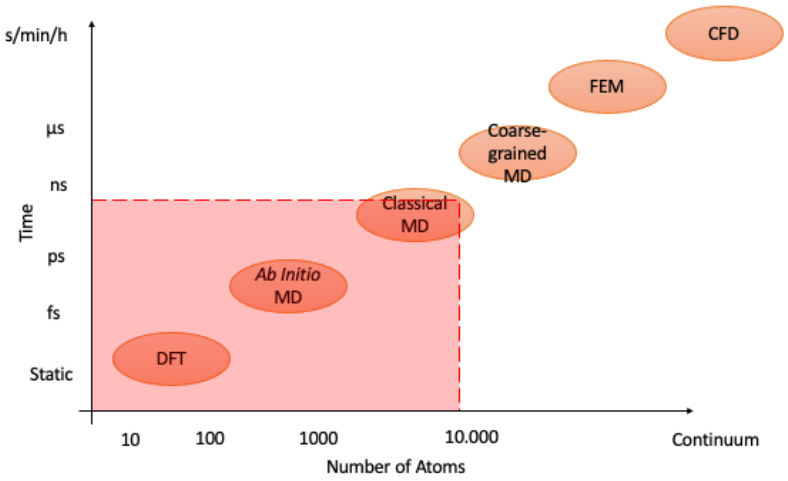

Figure 2.1: A sketch of some computational methods and the length and time scales they operate on. The red area visualises the limits of this thesis.

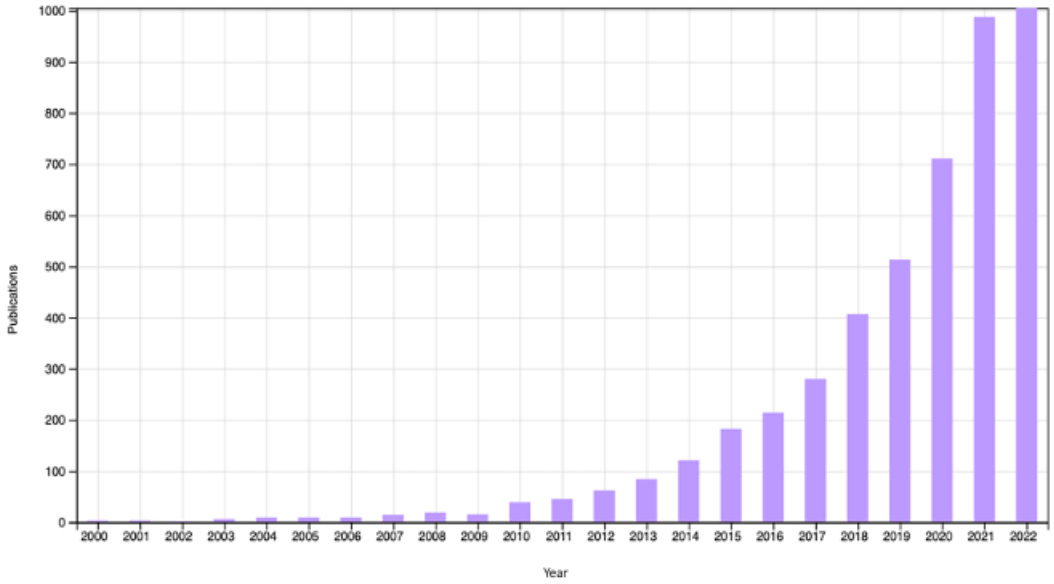

Figure 2.2: Number of academic papers between 2000-2022 that have both the key words "DFT" and "Batteries". [search 2023-05-01 using `www.webofscience.com`].

2.1 Density Functional Theory

In paper **I** the local bulk structures in electrolytes were studied at the molecular level using DFT calculations, in order to supplement and explain experimental data. For battery research purposes, especially for electrolytes, and in this thesis in particular, DFT is the method that is used to simulate the smallest scale of interest. The interest in using DFT to study batteries more or less started for real in the early 2000's (Fig 2.2) [22] and has since then manifolded.
The basis of DFT and similar methods can be described as follows: in order to describe a system from first principles we have to solve the Schrödinger equation:

$$H\Psi(r,t,\sigma) = i\hbar\frac{\partial\Psi(\vec{r},t,\sigma)}{\partial t}$$

where Ψ is the wavefunction describing the system, H is the system's Hamiltonian, $\vec{r} = (x,y,z)$ all coordinates describing the system, and σ is the spin of the system. Neatly packaged like this it is easy to think that all physics is solved, but as previously stated the many-body-interactions necessary to describe a system quickly become too complex to be solved for systems larger than the hydrogen atom. Hence if we want to understand complex materials from first principles approximations of both the Hamiltonian and the wavefunction are needed to perform these calculations *e.g.* the Born-Oppenheimer (BO) approximation.
Since a true representation of the wavefunction cannot be replicated on a classical computer due to the inability to store a true representation of the wavefunction in memory of a reasonable size [23], the first hurdle to overcome is to find an accurate representation of a wavefunction that we can work with. Oftentimes single-electron

wavefunctions, and molecular orbitals Φ_n are written using a basis set of functions φ_μ centred on the nuclei. The basis set functions are often a linear combination of Gaussian functions

$$\varphi_\mu = \sum_\mu d_\mu g(\xi, r)$$

where d_μ is a scale factor and

$$g(\xi, r) = Cx^{n_i} y^{m_i} z^{l_i} e^{-\xi_i r^2}$$

where C is a normalisation constant, n_i, m_i, l_i determines the type of orbital the function represent (s, p, d, etc.). Following the creation of a basis set ($\{\varphi_\mu\}$) molecular orbitals can be defined as:

$$\Phi_k = \sum_\mu c_{k,\mu} \varphi_\mu$$

Solving the Schrödinger equation is done through iteratively making better guesses for the wavefunction $\Psi(r_1, r_2, \ldots, r_n; R_1, R_2, \ldots, R_N) = \sum_k a_k \Phi_k$. What is solved for are the values of all coefficients a_k, enabling the energy $\epsilon = \langle \Psi | H | \Psi \rangle$ to be calculated. Since the variational principle states that $E_0 < \epsilon$, where E_0 is the system's ground state energy, it is possible to systematically find solutions of the wavefunction better able to recreate the ground state using an array of methods.

In this thesis DFT in a broad sense has been used to evaluate the energy and interaction forces in all systems studied. A quick introduction to the machinery; DFT utilises two theorems postulated by Hohenberg and Kohn [9], and is capable of identifying a system's ground state through the electron density rather than its wavefunction, reducing the number of coordinates needed to describe the system from $3(n + N) - 6$ to 3.

The two Hohenberg-Kohn theorems are:

1. *The ground state electron density uniquely determines the external potential of the system, and thus the whole Hamiltonian.*
2. *A universal functional, valid for any external potential, can be defined in terms of only the electron density.*

Using these two theorems the energy of the ground state of a system can be calculated from the electron density, and from the energy the force on all particles in the system follows. Important to understand how to evaluate system energy is the exchange-correlation potential $V_{xc}[n(r)]$ which is approximated by various functionals [24]. In paper **I** the Minnesota functional M06-2X [25] has been used in conjunction with the B3LYP functional [26]. The Minnesota functionals are a group of parametrised exchange correlation energy functionals, based on the meta-GGA exchange-correlation functional approximation meaning they include terms including the energy density, its first and second derivatives as well as being a hybrid functional meaning they also include parts of the exact exchange. B3LYP on the other hand is a less complex, GGA correlation function, simply containing information of the

energy density and the first derivative. Eventually in the final version of paper In papers **II** - **V** the PBE [27] functional has been used, which is a nonempirical GGA functional, making the approach truly general.

Even though DFT is considered accurate the method has drawbacks; The computational cost scales near cubically with the number of atoms in the system, making simulations of a single solvation shell the most common in the field of electrolytes. These typically target properties such as HOMO/LUMO levels, vibrational modes and frequencies, and their associated IR intensities as well as Raman activities *etc.* If we want to examine larger systems other methods are needed.

2.2 Molecular Dynamics

When large scale molecular bulk simulations are of interest MD is a great tool to both explain and predict electrolyte properties. Using a similar method as for DFT, we find that MD has been of interest to battery scientists since the mid 1990's [28]. MD in its most basic form is the solving of Newtons equations of motions for a many body system, which sounds simple enough. The interesting science lies in understanding how the atomic positions should be updated. One of the most common algorithms for updating positions in MD methods is the Velocity-Verlet algorithm [24]. Updating positions with a half-step the algorithm looks as follows:

1. $\vec{v}(t+\frac{1}{2}\Delta t) = \vec{v}(t) + \frac{1}{2}\vec{a}(t)\Delta t$
2. $\vec{x}(t+\Delta t) = \vec{x}(t) + \vec{v}(t+\frac{1}{2}\Delta t)\Delta t$
3. Derive $\vec{a}(t+\Delta t)$ for the updated positions $\vec{x}(t+\Delta t)$
4. $\vec{v}(t+\Delta t) = \vec{v}(t+\frac{1}{2}\Delta t) + \frac{1}{2}\vec{a}(t+\Delta t)\Delta t$

Where step 3 is non-trivial. In order to update the atomic positions the force acting on the atom has to be identified. Classical MD calculate the interatomic forces using a FF, which is a set of parameters and functions, together forming a potential energy surface where the total system energy is determined by the atomic positions $\left\{\vec{R}_j\right\}$. The energy is most often given by, but not limited to the form:

$$E_{tot} = 4\sum_{ij}\epsilon_{ij}\left[\left(\frac{\sigma_{ij}}{r_{ij}}\right)^{12} - \left(\frac{\sigma_{ij}}{r_{ij}}\right)^{6}\right] + \frac{1}{4\pi\epsilon_0}\sum_{ij}\frac{q_i q_j}{r_{ij}}$$
$$+ \sum_{\text{bonds}}\frac{k_b(l-l_{0,b})^2}{2} + \sum_{\text{bond angles}}\frac{k_a(\theta-\theta_{0,a})^2}{2} + \sum_{\text{dihedrals}}\sum_{n}k_{n,d}\cos(n\varphi+\varphi_{0,n}).$$

where the first term is the Lennard-Jones (LJ) approximation describing the Pauli exclusion principle and the van der Waals interactions, the second term is the Coulomb interaction between all pairs of atoms. Term three to five are all bonded interactions modelled as Hooke's law for two body objects, an angle potential defined by the angle between three bound bodies, and a proper/improper torsion potential defined by the angle between the planes formed between four bonded atoms. This form for the energy term (Fig. 2.3) is used in common FFs such as Amber [29],

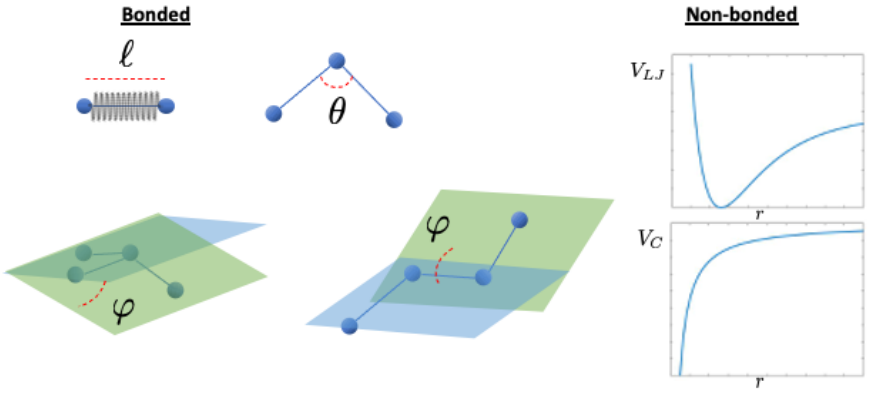

Figure 2.3: Schematic of bonded and non-bonded parameters making up a classical FF.

CHARMM [30], and GROMACS [31]. From this form the FF parameters are the set of $\{\epsilon_i, \sigma_i, q_i, k_{b,i}, l_{0,b,i}, k_{a,i}, \theta_{0,b,i}, k_{n,d,i}, \varphi_{0,n,d,i}\}$ where $\sigma_{ij} = \frac{\sigma_{ii}+\sigma_{jj}}{2}$, $\epsilon_{ij} = \sqrt{\epsilon_{ii}\epsilon_{jj}}$, and σ_{ii} is the distance at which the particle-particle potential energy is zero, ϵ_{ii} is the depth of the potential well. Conventionally FF parameters are developed using a combination of quantum chemistry computations of single molecules in vacuum, and experimental data, often of thermodynamic nature. However, since FF parameters are often validated by their ability to predict thermodynamical properties through experimentally obtained values it is not guaranteed that a given FF accurately represents local dynamics, even if the parameter set accurately recreates experimental values.

Conventional FFs as the ones discussed here also come with the drawback that all molecules are fixed, hence it is impossible to model chemical reactions this way, limiting for example the study of SEI formation. There are reactive FFs such as ReaxFF [32], whose parameter set can be extended to suit battery electrolytes [33]. However this is time consuming and this type of methodology also demands an extensive training set fully covering the relevant chemical space including activation and reaction energies, equations of state, surface energies, bond and angle stretches, and much more [34].

2.2.1 *Ab Initio* Molecular Dynamics

As mentioned above the most important step in an MD simulation is the identification of the forces acting on all particles in a system. An alternative method to the previously discussed FFs which is suitable when a higher level of accuracy is needed or when such FFs simply does not exist is to evaluate the forces acting in the system through quantum mechanical means.

The Hellmann-Feynman theorem shows that the force acting on a particle i is simply determined by the electron density as well as the Coulomb interaction between the nuclei:

$$F = -\frac{\partial E}{\partial R_i} = -\left\langle \Psi \left| \frac{\partial H}{\partial R_i} \right| \Psi \right\rangle = Z_i \left(\int n(r) \frac{r - R_i}{|r - R_i|^3} \mathrm{d}r - \sum_{j \neq i}^{N} \frac{Z_j (R_j - R_i)}{|R_j - R_i|^3} \right).$$

Therefore using similar methods for identifying the electron density as in DFT all forces acting within the simulation system can be identified. Knowing all the forces, the system can be propagated through time by solving Newtons second law, and updating all particles position, exactly as in the classical case. Deriving new accelerations at each iteration means solving a conventional matrix diagonalisation for an updated electron density with each updated position, as is done when using Born-Oppenheimer molecular dynamics (BOMD). This is computationally expensive when done at every time step, making this approach risible for even moderate scale systems [24].

An alternative approach to combine the quantum mechanical way to derive the forces acting in the system with classical MD was done by Car and Parrinello in 1985 (CPMD) [35]. This methodology has been used extensively in this thesis. However there are many other methods in between BOMD, and classical MD that solve a similar problem as CPMD such as Density Functional Tight Binding (DFTB) [36], Extended Tight Binding (xTB) [37], and Gaussian Plane Wave method (GPW) [38] just to name a few.

When running CPMD the total energy in a system is treated as a functional of the electronic wave function and nucleic positions:

$$E_{tot} = E_{tot}[\{\psi_i\}, \{\vec{R}_j\}].$$

From this separation, in combination with the fact that the electronic wavefunctions are orthonormal $\langle \psi_i | \psi_j \rangle = \delta_{ij}$ Car and Parrinello were able to compute the total energy using the variational principle. Hence $E_{tot}[\{\psi_i\}, \{\vec{R}_j\}]$ is minimized by varying the nucleic position simultaniously as the electronic orbitals, instead of computing the electronic structure at every MD step. In order to propagate the system in time and give the electrons a kinetic energy, a fictitious time dependence is given to the wavefunction, which allows the following classical Lagrangian to be constructed:

$$L(\{\psi_i\}, \{\vec{R}_j\}) = \frac{\mu}{2} \sum_{i=1}^{n} |\dot{\psi}_i|^2 + \frac{1}{2} \sum_{j=1}^{N} M_j \dot{\vec{R}}_j^2 + E_{tot}[\{\psi_i\}, \{\vec{R}_j\}] + \sum_{kl} \Lambda_{kl} \langle \psi_k | \psi_l \rangle$$

where μ is a fictitious electron mass. The fictitious mass should be small enough such that the Born-Oppenheimer approximation still holds and the electronic wavefunction adapts to the position of the nuclei, whilst at the same time being large enough to allow for relatively large time steps. A typical choice for $\mu = 400\ m_e$, which is what have been used in the calculations performed for this thesis. Beyond the introduction of a fictitious mass, Lagrangian multipliers Λ_{kl} are introduced as to fulfil

any external constraints, *e.g* retaining orthonormality of the Kohn-Sham orbitals at each time step. Solving for the classical equations of motion yield:

$$\mu\ddot{\psi}_i = -\frac{\delta E_{tot}}{\delta \psi_i} + 2\sum_j \Lambda_{ij}\psi_j \tag{2.1}$$

$$M_j\ddot{\vec{R}}_j = -\frac{\delta E_t ot}{\delta \vec{R}_j} + \sum_{kl} \Lambda_{kl}\frac{\delta \langle\psi_k|\psi_l\rangle}{\delta \vec{R}_j} \tag{2.2}$$

which are implemented in CPMD [39], the software used to generate data for analysis in paper **III**–**IV** and to generate training data in paper **V**.

2.3 CHAMPION

Even though MD techniques have been around for a long time there has not been a standard way of analysing the results. As stated by Hollingsworth and Dror [40]:

"The analysis process generally demands a careful combination of visual analysis using molecular rendering software and quantitative analysis. A number of common analyses are "pre-packaged" in readily available software, but most simulation projects benefit substantially from writing customized analysis programs or scripts, a task simplified by several analysis software frameworks."

There are some analysis tools that are used out there but in the author's personal opinion none has been sufficient to provide complex information about structure, transport properties, and similar, and too much time has been spent writing *"customized analysis programs"*. In paper **II** we present a bottom-up, generalised approach to analysing MD trajectories based on dynamic structure discovery (DSD). The DSD method works on finding out what species move together, and from those create a time dependent bond graph. This output can then be analysed based on the identified structures using graph theory and calculate physicochemical properties of said structures using statistical physics (Fig. 2.4).
The first step of the DSD is to automate bond detection. Our algorithm (pat. [41]) detect these by first identifying a list of candidate bonds, and then subjecting these candidates to a series of tests. The candidate bonds are identified through locating the pairs of atoms which are closer than a scaled sum of their atomic radii. The candidate bonds are only considered during the time while this criteria is fulfilled. During this time window the average atomic distance is computed, and if the pair is indeed bonded one would expect that their average distance over the bond lifetime is close to the pair types equilibrium bond length. The equilibrium bond length is also expected to be the most probable distance between two atom types. Hence we substitute the equilibrium bond distance by computing the partial radial distribution function (pRDF)

$$g_{ij}(r) = \frac{1}{n_0}\frac{n(r)}{4\pi r^2} \tag{2.3}$$

and recognising that the first peak corresponds to the most probable distance. $n(r)$ is the number density of neighbours of atom type j on a distance r from atoms of

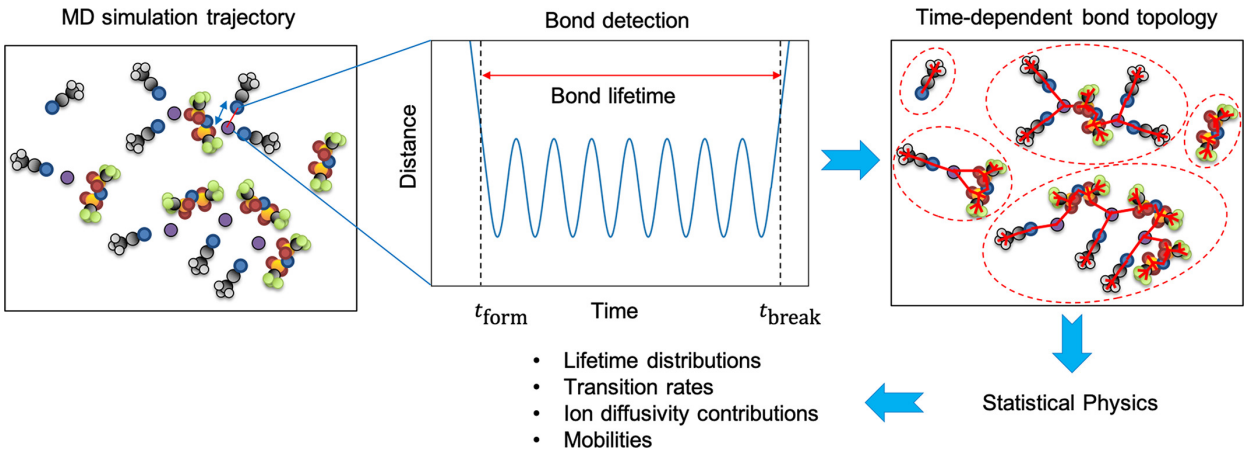

Figure 2.4: A schematic process of how the CHAMPION algorithm works [**II**].

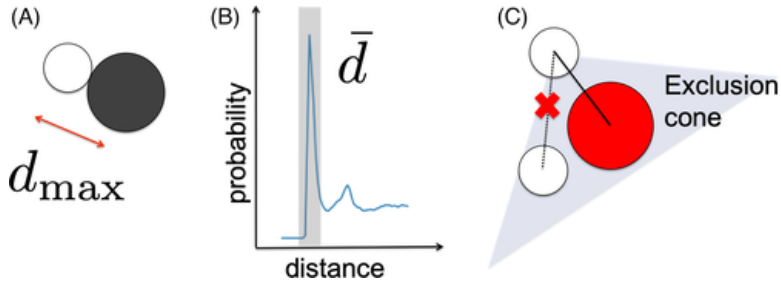

Figure 2.5: The basic criteria used by CHAMPION to detect and eliminate bonds [**II**].

type i, and n_0 is a normalisation factor corresponding to the average bulk number density.
The second test to determine a bond is whether or not the average distance is within a tolerance of this peak:

$$(1-\alpha)r_{peak} \leq \frac{1}{T}\int_{t}^{t+T} d_{ij}(t)\mathrm{d}t \leq (1+\alpha)r_{peak} \tag{2.4}$$

with α being the tolerance is proportional to the width of the pRDF peak.
Lastly the third and final requirement on a candidate bond we define in paper **II** is that the bond might not fall within an exclusion cone of a centrally bound species, *e.g* H-H in H_2O might fulfil the two first criteria, whilst we know they are both bonded to the O. Hence this is designed to eliminate false positives among the candidate bonds (Fig. 2.5).
When a candidate bond is accepted as a true bond the time for its formation and breakage times are recorded. These times are determined by measuring the time when the amplitude of the sinusoidal oscillation around the bond length equilibrium goes below, for formation, and above for breakage, the furthest distance during oscillation. The furthest distance is the equilibrium bond length plus the amplitude of the oscillation (Fig 2.4).
Using this bond detection algorithm provides all the information needed to create a time-dependent global bond graph, uniquely describing a systems bond topology.

The bond graph is an undirected labelled graph, with atoms describing the vertices, labeled either by atom type, or atom index, and the bonds represent edges. Worth noting however is that the edges are unlabelled since the algorithm does not make any distinction between bond order.
However having access to only the global bond graph does not allow one to compute physical properties. To identify the species in the global bond graph a modified version of the subgraph isomorphism algorithm presented by Bonnici et al. [42] is implemented in this thesis, expanding CHAMPIONS functionality. The subgraph isomorphism algorithm consists of four criteria that has to be fulfilled and applied to a search space tree (fig 2.6):

- Neither vertex u_i nor the matched vertex $M(u_i)$ are already matched in the current path.
- u_i and the matched vertex $M(u_i)$ are of the same type, *e.g.* both u_i and $M(u_i)$ are labelled as carbon.
- The number of edges connected to $M(u_i)$ in the list of vertices in the target graph, is equal to or greater than the number of edges connected to u_i in the list of vertices in the pattern graph.
- The topological constraint so far in the matched pattern are fulfilled.

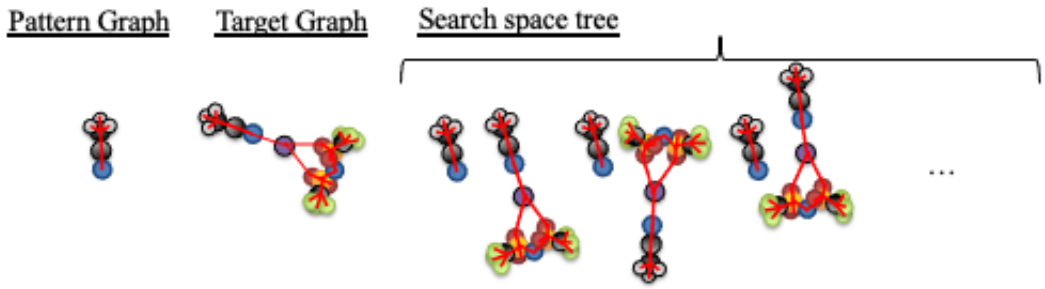

Figure 2.6: Showcasing a ACN pattern graph, a target graph, and a subset of the search space tree.

By treating a molecule as a subgraph it is possible to map all bonds and edges in the global bond graph to molecules. Hence we can automatically analyse all clusters based on the composing species. This facilitates calculating material properties using common statistical physics methods.

2.4 Machine Learning Techniques

With this strong push to understand complex materials such as new electrolytes another type of methods used to tackle this problem and a contender to simulations and CHAMPION has been machine learning (ML). With a recent surge in methods bridging the realm between AIMD and classical MD simulations, ML used to describe materials structure began in 2007 when Behler and Parinello [43] developed symmetry

functions (SF), creating transferable neural network (NN) potentials through the chemical locality around an element. Similarly in 2013, Bartók et al. developed the Smooth Overlap of Atomic Position (SOAP) directly defining the similarity between any two atomic neighbourhood environments, enabling the development of interatomic potentials through the GAP framework [44], [45]. Other alternatives to develop interatomic potentials have been through different NN approaches, such as SchNet [46]. More concretely relevant for electrolyte
applications, Wang et al. for example have developed a NN based on SchNet, learning chemical embeddings for elements in ionic liquids and new electrolytes [47]. Alternatively NN such as PiNet [48] can be used to learn electronic multipoles of atomistic simulated liquids [49]. Worth noting is that most common ML approaches work best for structured materials such as crystals, where it is much easier to locate a good descriptor of the local structure. Comparatively it is much harder to get equally good results for amorphous materials such as electrolytes due to the non periodic behaviour of these materials. Anyhow, notable progress have been made in recent years [50], [51].

2.4.1 Neural Networks

As noted above, NN are a popular choice when attempting to predict materials properties since it has a good ability to find patterns in data that is hard to analyse by humans. This thesis will not attempt to be a be all end all source of information regarding NN's, however it is important that we all have a basic understanding of the fundamentals.
At its' core NN attempt to replicate the way the human brain functions through replicating the behaviour of biological neurons. The artificial neuron takes one or more inputs and produces a single output. To produce this output a weighted sum of all the inputs is taken and then a bias term might be added. This sum is sometimes referred to as the *activation*. The activation is then passed through an activation function, which in its' simplest form can be linear, but usually is not. The inputs to a neuron is oftentimes outputs from other neurons, forming a network of connected neurons with an input layer and an output layer, and one or several hidden layers in between. Concretely for the interest of material scientists NN used in this way is a great tool to identify a connection between a chemical environment, as e.g. described by SOAP [45] and forces for atomic modelling as has been done previously in literature [52].
To train a NN the weights and biases of all the neurons are updated based upon how well they fit data and training is considered done when additional data does not significantly lower the error. Common for almost all ML approaches, especially those based on NN is the need for extensive amounts of data for training and testing of models, making the need for available data more important than ever. This need can be seen in contemporary projects such as BIG-MAP [53] as well as the Materials Genome Initiative [54] trying to standardise data presentation as well as making it available to a wider audience.
The use of NNs to aid the development of MD methods have been a topic of interest

for material scientists in recent years. One example of how this can be done is found in Wang et al. [55] where, using differentiable simulations, they are able to obtain interaction potentials, through the use of gradient decent. This aim is similar to the one which we are trying to solve later on in this thesis using our own method.

2.4.2 Genetic and Evolutionary Algorithms

Another interesting ML technique is Genetic Algorithms (GA). Like NN GA also tries to replicate a biological phenomenon, this time replicating the process of natural selection [56]. Hence GAs belong to a larger class of ML techniques called Evolutionary Algorithms (EAs). Like in the case of NN, this thesis will only present the reader with a short introduction to the topic.
EAs are good optimisation heuristics for problems where an optimisation has to be done involving conflicting objectives or a high-dimensional search space [57]. Due to a large search space of solutions to such a problem it is often extremely hard to find an optimal solution. Nevertheless in practice it is often viable to simply find a solution that is similar enough to the optimal solution to be a feasible approximation, or in laymens terms “good enough”.
EAs are implemented by initialising a population of possible solutions to the problem. Each solution is reffered to as an individual. Every individual is evaluated according to some cost function and the n individuals with lowest cost are selected for ”breeding”. There are several different methods for generating the next generation, but in general it involves some kind of crossing over or other recombination of “parents” genes. This is done with the hope that some of the recombined offspring will yield a result with an lower cost than the previous generation. It is however impossible to cover the full search space by just recombining the initial population set [58]. To enable the method to cover all possible solutions and prevent ending up in local minimum the concept of mutation, a small perturbation to one of the "genes" in the individual is introduced. A gene here refers to one of the values making up the individual, and this perturbation slightly alters the solution enough to cover the full search space. The consecutive generation generated is then evaluated against the cost function in turn, and the process is repeated iteratively until a sufficient answer is provided according to some cost function.
It is worth noting that this thesis is sprung from the author’s failed attempts to generate classical FF parameters from AIMD simulation data during his master thesis. These attempts were substituted by the approach presented in **2.6**.

2.4.3 Gaussian Process Regression

A final ML method I want to touch upon in this chapter which is good for interpolation of data given a sparse set of data points is Gaussian Process (GP) regression, commonly known as Kriging, which is used to supplement the method elaborated upon in **2.5**. Given a suitable choice of prior GP regression gives the best linear unbiased prediction at unsampled locations. GP regression is used to predict a function value at a given point by computing the weighted average of the known values of the function in the neighbourhood of the point. This means that a GP is

completely specified by a mean function and a positive definite covariance function. Given a set of inputs $x^{(1)} \cdots x^{(n)}$, a mean function $\langle f(x) \rangle = 0$, and a covariance function $K_{p,q} = \mathrm{Cov}\left(f(\mathbf{x}^{(p)}), f(\mathbf{x}^{(q)})\right) = K\left(\mathbf{x}^{(p)}, \mathbf{x}^{(q)}\right)$, a joint distribution may be defined

$$f(\mathbf{x}^{(1)}) \cdots f(\mathbf{x}^{(n)}) \sim \mathcal{N}(\mathbf{0}, K).$$

Given this knowledge a GP can be obtained using Bayesian linear regression:

$$f(\mathbf{x}) = \mathbf{x}^T \mathbf{w}$$

where the weights $\mathbf{w} \sim \mathcal{N}(\mathbf{0}, \Sigma_p)$. Hence the mean function is given by:

$$\mathbf{E}\left[f(\mathbf{x})\right] = \mathbf{x}^T \mathbf{E}[\mathbf{w}] = 0$$

and the covariance function is given by:

$$\mathbf{E}\left[f(\mathbf{x}) f(\mathbf{x}')\right] = \mathbf{x}^T \mathbf{E}[\mathbf{w}\mathbf{w}^T]\mathbf{x}' = \mathbf{x}^T \Sigma_p \mathbf{x}'.$$

The Bayesian linear regression is based on Bayes theorem:

$$P(\mathbf{y}|X, \theta) \propto P(\theta) P(\theta|X, \mathbf{y})$$

Where $P(\theta)$ is known as the prior, representing the assumption of the probability of a set of parameters θ prior to knowledge of data, and $P(\theta|X, \mathbf{y})$ is known as the likelihood, representing the probability of observing the parameters θ given knowledge about the data $X, \mathbf{y}$, and $P(\mathbf{y}|X, \theta)$ is the posterior of the given hypothesis explaining the data. Commonly θ is chosen by optimising the marginal log-likelihood:

$$\log P(\mathbf{y}|X, \theta) = -\frac{1}{2} \log |K(X, X) + \sigma^2| - \frac{1}{2} \mathbf{y}^T (K(X, X) + \sigma^2)^{-1} \mathbf{y}$$

through sampling the probability space of possible θ.

2.4.3.1 Choice of Priors

The prior, or prior probability distribution, is the assumed probability of a data set before any observations is taken into account. There are many ways to determine a prior, it can be constructed from past experiments or samplings if information is available, or from the subjective assessment of a researcher. With no information available it can also be based on the principle of indifference giving an equal prior probability to every possibility.
A informed prior assumes explicit information about the variable studies. A good example is to assume a process is a Gaussian distribution around some known mean. On the other end of prior knowledge, the uninformed prior makes little to no assumption about the variable, but can still make general statements such as "the variable is positive". Oftentimes this just assigns equal probability to every possibility.

2.4.3.2 Kernels

At the heart of the GP regression is the GP kernel. The kernel function $K(X_i, X_j)$ essentially tells the model how close two points (X_i, X_j) are. There are several kernel functions available and the choice should be made based on what data is studied. The default kernel used by many machine learning libraries (e.g. scikit-learn as used in this work [59]) is the radial basis function kernel (also known as the quadratic exponential kernel, the squared exponential kernel or the Gaussian kernel) with the form:

$$K(X_i, X_j) = \mathrm{e}^{-\frac{||X_i - X_j||^2}{2L}} \tag{2.5}$$

where L is the length scale of the system, and is popular because of its ready interpretation as a similarity measure ranging from one when $X_i = X_j$ and zero in the limit. Generally this model will not be able to make predictions further than a distance L away from the training data which limits its applicability if the sample space is small.
Other notably common kernals are the white noise kernal ($K(X_i, X_j) = \delta_{ij}\nu$, where ν is some noice level) and the constant kernal ($K(X_i, X_j) = \kappa$, where κ is some constant). In the work done throughout this thesis, and more specifically the work done in **2.5** the Rational Quadratic kernel (RQK) has been used.
The RQK is equivalent to the summation of multiple radial basis function kernels of different length scales:

$$K(X_i, X_j) = \left(1 + \frac{||X_i - X_j||^2}{2\alpha L}\right)^{-\alpha} \tag{2.6}$$

where L is yet again the kernel length scale, and α is the weighting of importance of different length scales in the kernel. The RQK was chosen since it is a simple enough function to use on this data set where we do not expect any discontinuities and it is commonly used to great success in a vide variety of cases [60].

2.5 Curve Smoothing via Kernel Smoothing

An alternative way of obtaining a curve from data is using a smoothing function, especially a kernel smoothing. A kernel smoothing is a moving average smoother using a kernel weight function, to give an average estimate of a real valued function in every observable point. There are many different kernels, some of the more common ones being Gaussian, squared exponential, and nearest neighbour kernel. Within this thesis kernel smoothing is used as an alternative approach to GPR. Kernel smoothing is based on:

$$\hat{Y}(X_0) = \frac{\sum_{i=1}^{N} K(X_0, X_i) Y(X_i)}{\sum_{i=1}^{N} K(X_0, X_i)},$$

where $K(X_0, X_i)$ is a kernel, N is the number of observed points, and $Y(X_i)$ are the observation at point X_i, which gives us the smoothed function $\hat{Y}(X)$. From this the advantages of a non-parametic function estimator emerge which can uncover

structural features in data which a parametric model might not reveal. The main drawback is that this type of model does not provide any parametric model to describe the data.

2.6 Automated Force Field Finder

2.6.1 Background

To tie all of this together I now want to present the original idea for CHAMPION, which was a two pronged spear, one part consisting of the DSD functionality, the second part was to enable longer and more accurate MD simulations. To allow this one must be able to describe a Hamiltonian that can be parametrized to reproduce empirical data as well as possible, whilst still being parametrized in a way that makes it computationally inexpensive.
The first attempt was to match classical FF parameters to AIMD forces using GAs. However, it was discovered that the parameter space, with a roughly fifty or more parameters, seemed too large for a GA to fit, or the cost function space to shallow to find a good solution. This was exemplified by that the algorithm identified widely different solutions at the same cost (Table 2.7) [61].

Table 2.7: The Hooke's force constant k_{ij} with the interaction force centre types.

Force Centre Type	FF1 [kJmol^{-1}nm^{-2}]	FF2 [kJmol^{-1}nm^{-2}]	FF3 [kJmol^{-1}nm^{-2}]
0,2	916.48	5451.75	3807.14
1,3	13848	18981.5	12150.5
0,1	3510.6	3614.1	2263.55
5,7	2075.4	5390.7	6766.7
5,6	2403.6	123.001	2686.92
6,9	4079.5	8629.06	6526.38
6,8	6603.7	10432.2	14607.4

In paper **V** we propose a new light-weight method for generating system specific FFs. Being inspired from the work of Åvall and Johansson (2020) [20] where they investigated the force distribution between a solvation shell and a central atom in terms of centre-of-mass coordinates, we herein develop a similar method by generalising the Åvall method of binning central forces depending on distance to binning the interaction strength related to each interaction type. We are able to use this method to develop a FF due to the fact that a system can be completely determined by knowledge of all correlation functions $g^{(n)}(x_1, ..., x_N)$ [62].
The interaction types used are the same as in conventional FFs, with 2-, 3-, and 4-body bonded interactions, as well as an electrostatic term and a Lennard-Jones like term. In this method however the long range electrostatic and dispersion interactions are treated together and will henceforth be referred to as the pairwise interaction. By first running small first principle MD simulations, the forces acting between all particles of a system type can be found.

Then projecting the generalised force acting on all particles partaking in an interaction type based on a CHAMPION bond graph, against a generalised coordinate q describing said interaction, a 2D histogram of distributions (Fig. 2.8) are formed.
The force projection is obtained through the virtual work, giving us the following conversion between a general force Q_j and the carthesian force $\vec{F}_i$:

$$Q_i = \sum_{j'=0}^{N} \vec{F}_j \cdot \frac{\partial \vec{r}_j'}{\partial q_i}, \tag{2.7}$$

, q_i is described by the internal coordinates displayed in fig. 2.3.

2.6.2 Wilson Theory

The object $\frac{\partial \vec{r}_i}{\partial q_j}$ is hard to calculate. However the context of internal molecular coordinates, the derivation of internal coordinates with respect to Cartesian coordinates are well defined and this transformation matrix is called the Wilson's **B** matrix [63]:

$$B_{ij} = \frac{\partial q_i}{\partial R_j} \tag{2.8}$$

where $q_i, i = 1 \dots M$ are still the internal coordinates and $R_j, j = 1 \dots 3N$ are the Carthesian atomistic displaysment coordinates. These internal coordinates are the same as the ones discussed in **2.2**, known as the *natural internal coordinates*, and unlike the coordinates of the Z-matrix this coordinate system is redundant. This allows us to perform a transformation from cartehsian coordinates, to internal coordinates, and back, making this method easy to automate.
From the Wilson's **B** matrix and it's pseudo inverse it is possible to generate a transformation between Carthesian coordinates and the redundant internal coordinates:

$$\mathbf{A} = \mathbf{B}^T(\mathbf{B}\mathbf{B}^T)^{-1} \tag{2.9}$$

or

$$\mathbf{A} = (\mathbf{B}^T\mathbf{B})^{-1}\mathbf{B}^T \tag{2.10}$$

depending on if **B** is full row rank, or full column rank, where $\mathbf{BA} = \mathbf{I}/\mathbf{AB} = \mathbf{I}$ (from here on out we will concider **B** to be full row rank). It follows that eq 2.7 can be rewritten as:

$$\mathbf{Q} = \mathbf{FA} \tag{2.11}$$

where **F** is a flattened $(1 \times 3N)$ vector of $\vec{F}_i$.

2.6.3 The Åvall Method

These 2D histograms contain all information about said effective interaction, *e.g.* between two carbon atoms, where effective interaction denotes the distributions of interactions in the presence of environmental noise assumed to be normally distributed with zero mean. Having this method based upon the CHAMPION bond-graph identifying method [**II**] also enables a FF that treats different bond

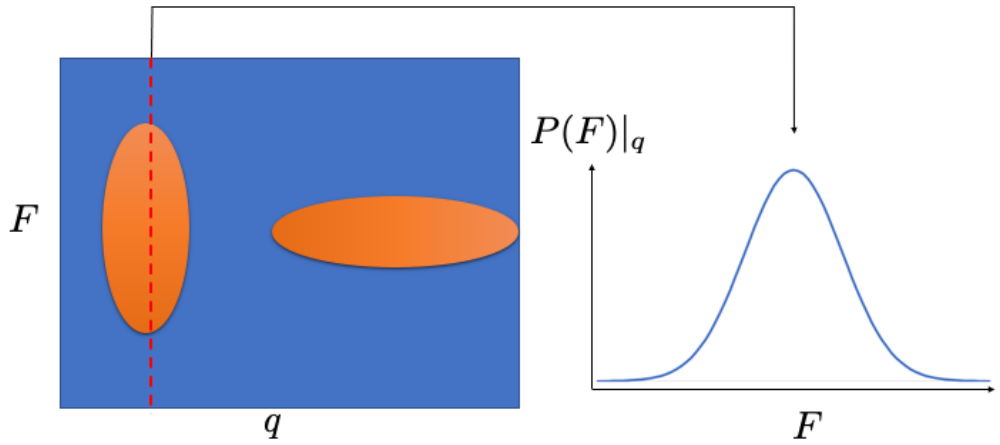

Figure 2.8: Schematic Åvall plot linking the probability distribution of generalised forces to a generalised coordinate describing a interaction. Orange: Occupied bins. Blue: Empty bins

types separately, *e.g.* separating linearly bonded carbon from cyclically bonded carbon. Such distinctions have been shown to be useful in other, more conventional, FFs such as AMBER and GROMACS [29], [31].

From the positions of and forces acting on each atom, both the generalised coordinates and forces can be computed and sampled. The statistical distributions of generalised forces as functions of the corresponding generalised coordinates result from a combination of the effective interaction between the atoms involved, and effects of the background. The approach taken here is based on assuming the background effect to be unbiased noise, so that the mean of the sampled distributions estimates the true effective interaction.

Knowing the positions and forces acting on each particle within a trajectory, generalised coordinates and generalised forces can be computed and sampled. The distributions of generalised forces as function of the corresponding generalised coordinates give rise to a 2D histogram similar to an Åvall plot. These histograms contain the information about the effective interaction between all particles involved, as well as the effective background.

Given a force distribution $\mathcal{F}|_q$ of generalised forces $\{F_i(q)\}$ as seen in Fig. 2.8, where $i \in \{0, \text{number of samples of interaction type}\}$ one can show that the specific force $F_i(q)$ can be written as:

$$F_i(q) = F(q) + \Delta f$$

where $F(q)$ is the true generalised interaction strength and Δf is a stochastic

background noise. Assuming that the noise is Gaussian:

$$\begin{aligned} \sum_i^N F(q) &= \sum_i^N F_i(q) - \sum_i^N \Delta f \\ &\Rightarrow \\ NF(q) &= N\left\langle F_i(q)\right\rangle - N\left\langle \Delta f\right\rangle \\ &\Leftrightarrow \\ F(q) &= \left\langle F_i(q)\right\rangle . \end{aligned}$$

Hence on a global level the background of forces along a generalised coordinate q cancel out. From this we make the assumption that the true force of q can be described by the mean force curve. Hence any interaction described using the generalised Åvall method should be reproducible given the mean force value at any point along the generalised coordinate axis.

Given the sparse but spread out nature of the data produced this way, a smooth function filling the space between data points can be generated using GP regression. This pairs well with the reactive capability provided by having the method based upon the CHAMPION method. The FF identified can be made reactive through computing bond likelihood functions as a function of distance. Hence it is possible to determine on a snapshot-by-snapshot basis which atoms in the system are bonded in, one, two, three, or even four of the four bond types previously discussed. This possibility enables the look-up tables to be dynamically chosen during the simulation, enabling a great amount of customiseability to the interactions.
Hence we have proposed a novel system building on the descriptors identified by CHAMPION that enables a quick and lightweight way to evaluate interatomic forces using a conventional FF parameter model.

3
Battery Electrolytes

In a battery the role of the electrolyte is to transport ions from the positive to the negative electrode, and back during cycling. In order to do this effectively the electrolyte is required to have a high ionic conductivity in the temperature range of the application [64]. In order to allow for electrochemical cycling the electrolyte also has to be electronically insulated, forcing electrons to pass through an external circuit instead of through the electrolyte. Beyond these criterion a general "good" electrolyte also has to be thermally, chemically, and electrochemically stable within the operating voltage window, which normally lies between 0-5 V vs. $M^{x+}/M^{\emptyset}$[65]. Then comes the wish list that takes more humane values into account where we want an electrolyte to be non-toxic, using raw materials that are cheap and available, as well as being obtained from a non destructive production. Unfortunately there is as of 2023 no commercially available electrolyte that fulfils all criteria listed here. There are several different electrolyte concepts such as liquid electrolytes (LEs), solid state electrolytes, polymer electrolytes, and many more. All with their own advantages and disadvantages. In this thesis we will discuss LEs, highly concentrated electrolytes (HCEs), and localised highly concentrated electrolytes (LHCEs), a quick and non-comprehensive overview of some advantages and disadvantages are presented in Table 3.1.

Table 3.1: A list of the different electrolyte types touched upon in this thesis and a non-comprehensive summary of their advantages and disadvantages.

Electrolyte Type	Advantages	Disadvantages
LE	Low Viscosity, Good Wettability, Conductivity, ESW	High Flammability
HCE	Low Flammability, ESW, Rate Capabilities	High Viscosity, Low Conductivity
LHCE	ESW, Low Flammability, Low Viscosity	Highly fluorinated

3.1 Conventional Liquid Electrolytes

In a LIB the electrolyte, *e.g.* LP30, consists of solvents and a solute with the main purpose to transport charge carriers from one electrode to the other. Beyond the

general properties listed above it is important for a LE to have a low vapour pressure to ensure safety, and low cost etc. [65].
When designing a LE the choice of solvent is important in order to fully dissolve the salt. Hence important properties to keep in mind are a dielectric permittivity and a low viscosity, since a high permittivity is crucial in order to dissociate the salt, and a low viscosity correlates with good transport properties. In order to fulfil both these criteria several solvents are usually used, such as in the case of LP30, where equimolar parts of ethylene carbonate (EC), and dimethyl carbonate (DMC) are used. Worth noting however is that despite being one of the most popular commercial electrolytes available, there are still safety concerns regarding LP30, with both EC, and DMC being organic solvents, and being flammable and volatile [66]–[68]. Hence studies into other electrolyte concepts are needed.

In order to understand the charge transport in electrolytes, and hence being able to select for good properties, it is important to study the mechanisms that facilitate transport, and what structures enable transport. The net transport of charges is driven by the difference in electrochemical potential between the electrodes. Even though this is the driving force on a macroscopic scale it is important to keep in mind the importance of both time and length scale. Herein we will discuss the importance of understanding the electrolyte structure at different scales in order to explain behaviour. In a LE the local scale surrounding the cation is made up of the first and second solvation shells (Fig 3.2). The solvation shell is the result of solvent molecules arranging themselves around the positively charged ion. Since the cation, oftentimes Li^+ is small and spherically symmetrical the resulting electrical field is also spherically symmetrical, causing the nearby solvent molecules to align. Since the strength of the electric field decrease exponentially with the distance from the cation this ordering effect usually only works on one, max two layers of molecules, with the second layer being much less ordered than the first. These solvation shells are strongly cohesive and have long lifespans. In paper **IV** we study how the local solvation shell structure depend on salt concentration moving from LE to HCE using AIMD simulations and CHAMPION analysis. The results obtained using this method are more or less directly comparable with experimental structure studies, such as nuclear magnetic resonance (NMR) studies, and different scattering studies, *e.g.* using small-angle X-ray scattering (SAXS) [69], [70].

The work done in this thesis also touches upon the problem of finding a good electrolyte for calcium systems. Currently $Ca(BF_4)_2$ salt and carbonate solvent electrolytes show a large ESW. However these system require temperatures above 100 °C in order for the battery operation to be reversible [71]. Close to room temperature THF based electrolytes can used to produce operating Ca cells. These types of electrolyte come with the drawbacks that the anodic stability is low ($\sim$ 3 V vs Ca^{2+}/Ca) which limits the selection of high voltage cathode materials [72], in turn lowering the cell energy density. Hence a viable middle ground has to be developed in order to make Ca-metal batteries a commercial reality.

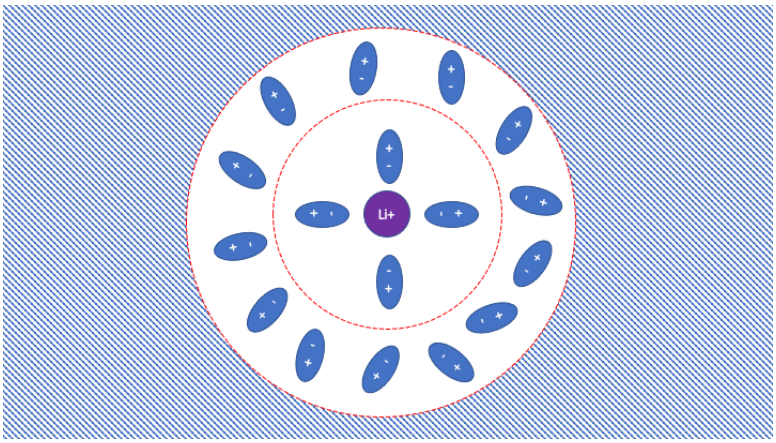

Figure 3.2: A schematic drawing of the first and second solvation shell in a lithium based LE. The red ring mark the border between the first and second solvation shell, and outside the second shell there is a homogeneous background medium.

3.2 Highly Concentrated Electrolytes

Conventional electrolytes, such as LP30, use salt concentrations around 1 M in order to maximise conductivity. However since the early 2010's the interest for much higher salt concentrations in battery electrolytes have increased dramatically, despite the dropp in conductivity seen above 1 M. The increased interest is due to some interesting properties displayed such as; a lower solubility of transition metals dissolving from cathodes [73], higher rate capabilities [74], [75], and a widened ESW [74], [76]. All these properties are attributed to the change in solvation shell structure around the Li-ion [77]. Since HCEs as a class seem to have many of these positive attributes, which to be achieved for in LE the solvent have to carefully selected, implies that the safety of HCEs can be increased by selecting less flammable solvents. These solvents might have been overlooked previously due to being bad electrode passivators, a property which in HCEs is achieved through the choice of salt. As an example McOwen et al. showed using a combination of Raman spectroscopy, electrochemical testing, and computational work that such HCEs are safer than LP30 [76].

The addition of more salt causes the electrolyte to have high ion density more akin to solvent in salt, than salt in solvent, making the electrolyte take on behaviour similar to ionic liquids [78], [79]. This also means that there is a low amount of free solvent in the liquid, which is one of the major identifiers of HCEs. However, as we show in paper **IV** the amount of free solvent molecules might not go to zero, but rather be caught up in a matrix of cations, anions, and interacting solvent molecules. Furthermore this structure leads to a higher density, higher viscosity, besides a lower total ionic conductivity. Using a combination of experimental techniques Nilson et al. have shown that ionic conductivity depends more strongly on ionicity than viscosity [80], which is in agreement with the argument by Seo et al. [81]. In paper **III** we describe the mechanism behind the lower ionic conductivity for lithium bis(trifluoromethanesulfonyl)imide (LiTFSI) in acetonitrile (ACN) at a 1 : 2 molar

ratio and show that a percolating network form from the anions and cations at such a high salt concentration whilst the solvent remains free. The lower ionic conductivity is explained by a decreased amount of transportation being conducted through a vehicular mechanism, which is defined as a cation in a shell of coordinated solvent molecules moving freely through the electrolyte (Fig. 3.3a), contrary to a higher amount of non-vehicular transport, which is all type of transport that is not vehicular. This could for example be structural deformation, structural rotation, or jumping (Fig. 3.3b).

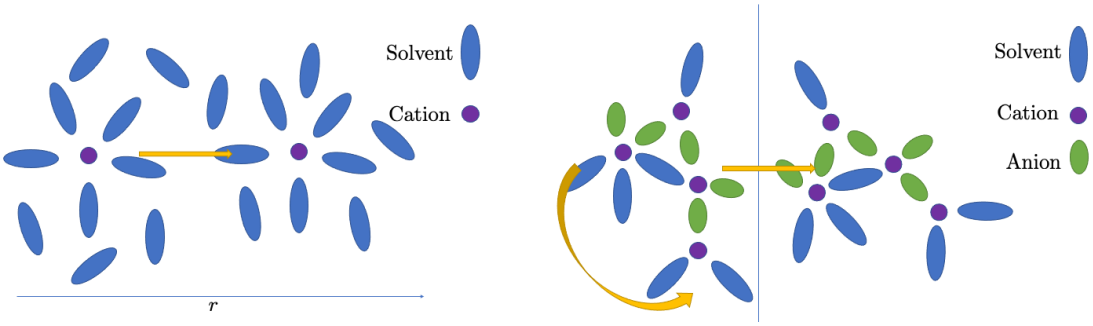

(a) How a solvent molecule shell forms a "vehicle" surrounding the cation and enabling transport through the solvent

(b) Rotating a structure containing cations can lead to a net charge transfer. This is an example of non-vehicular charge transfer.

Figure 3.3: Different charge transfer mechanisms at intermediate and high salt concentrations.

This view is coherent with experiments. Dokko et al. [82] showed through the use of NMR studies an unusually high lithium self diffusion in a sulfolane based electrolyte. This study show that lithium diffuse faster than both the solvent molecule and the anion, which clearly cannot happen if transport is vehicular, and they attribute the increased lithium diffusion to jump diffusion.

3.3 Localised Highly Concentrated Electrolytes

LHCE are designed to retain the positive qualities of HCEs, whilst improving the reduced ionic conductivity, and high viscosity, causing poor electrode and separator wetability, that comes with an increased salt concentration. Dilluting a HCE might sound counter intuitive, but if choosing the correct solvent the local highly concentrated behaviour can be retained. This is done by introducing a non-solvent, a diluent, keeping the 1st solvent shell of the cation of the HCE intact by the diluent being non-coordinating to both the cation and the anion. This, if done properly, lowers the viscosity, whilst retaining the positive properties from HCEs. Additionally, the diluent should be stable against other cell components [83]. Hence it is globally similar to a LE, but locally similar to a HCE. The diluent oftentimes are some kind of ether, particularly fluoroethers as seen in the works of Qian et al. [84], and Wang et al. [85], [86]. Given a shared local structure with HCEs the SEI forming abilities remain [87]. As recently seen the SEI formed from LHCE system are composed

mainly of species coming from the anion decomposition and (near the surface) from the decomposition of diluent as well [88], [89]. Hence decomposition will occur using these systems, and the diluent has to be chosen accordingly, increasing the complexity of choice for electrolytes. Given the correct choice of diluent a more stable can be created as shown by Ding et al. [90] where SEIs made from flourinated diluent decomposition on lithium metal has been shown to increase stability. It has also been shown that the correct diluent can decrease the dissolution of poly-sulfides into the electrolyte in Li-S systems [91]. All choices can be aided using computational means. For example: as preparatory work for paper **I** we screened many potential fluoroethers using DFT for their interaction energy against some standard acid in order to find out how inert their interaction is. Through this method a set of suitable candidates could be preselected and the scope of testing narrowed down. Similarly, MD is an additional method that could be used for screening. In 2020 Bouibes et al. [92] utilisedthe generalized AMBER forcefield GAFF to show the miscibility behaviour of a set of flourinated diluents and their ability to form LHCE structure. The importance of computational methods for investigating LHCEs are even higher than for other electrolyte types due to properties of the diluent, since many diluents contain high amounts of flourine and the F - F interaction are important for many properties of these types of liquids. These interactions are hard to probe spectroscopically, leaving computational methods as a more effective choice.

3.4 Ion Transport in Electrolytes

The primary function of a battery electrolyte is to facilitate ion transport, it is crucial to understand the transport mechanisms occurring within the electrolyte. A common liquid electrolyte cell works with a cell voltage of the order of magnitude of < 5 V, meaning that a Li^+ experiences an energy contribution of 5 eV. Operating at room temperature the thermal energy of the surroundings is $k_BT \approx 25$ meV. Hence, on a global scale bulk transport is driven completely by the electric field caused by the voltage difference between the electrodes. Focusing on a local scale however, assuming a thin separator (~ 20 μm) we see that linearly approximating cell voltage over separator thickness $\approx 2.5 \cdot 10^5$ Vm^{-1} over a typical distance of inter-molecular interaction (~ 5 Å), E = 0.125 meV (Fig 3.4). As a consequence the local dynamics is assumed to display motion uniformly distributed over all directions. In practice however the voltage profile is extremely steep near the electrode interfaces, making the importance of this potential more substantial there, and even less important than assumed here within the bulk, but that is outside the scope of this thesis.
The most important property for transport performance in a battery cell is the ionic conductivity σ of the charge carrier, defined by:

$$\vec{J}^+ = \sigma^+ \vec{E}$$

relating the current density $\vec{J}$ of the charge carrier to the applied electric field $\vec{E}$. Generally σ is a tensor, and using the Onsager transport coefficients, can be

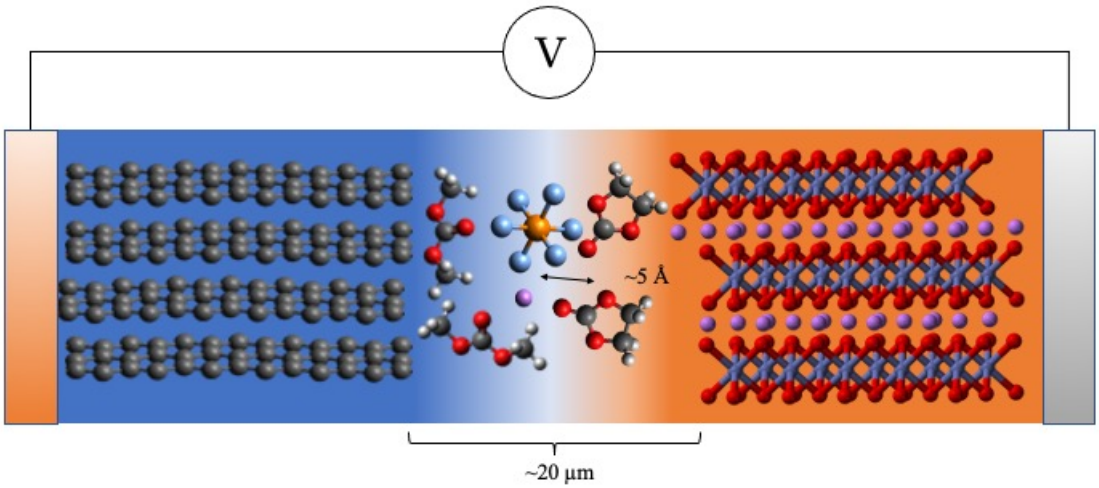

Figure 3.4: Sketch of a battery cell. Atoms are not to scale.

described as

$$\sigma = \sigma^{++} + \sigma^{--} - 2\sigma^{+-}$$

where σ^{++} is the cationic contribution, σ^{--} is the anionic contribution, and σ^{+-} is the cation-anion correlation term. For further insight into a materials transport properties these terms can be decomposed into self correlation, and distinct correlation contributions:

$$\sigma^{++} = \sigma^{+}_{\text{self}} + \sigma^{++}_{\text{distinct}}$$
$$\sigma^{--} = \sigma^{-}_{\text{self}} + \sigma^{--}_{\text{distinct}}.$$

Note that the self correlation is large when ions have high mobility, and the distinct correlation is positive when ions diffuse in the same direction, and negative if they diffuse in opposite directions. In isotropic media such as liquid electrolytes however the ionic conductivity tensor is reduced to a scalar.
Worth mentioning is that the species ionic conductivity is easy to calculate computationally it is harder to measure its analogue experimentally. More often the total ionic conductivity $\vec{J} = (\sigma^{+} + \sigma^{-})\,\vec{E}$ is reported when presenting experimental results, even though it is of lesser importance for battery performance. However there are several counter examples to this claim that calculate cationic and anionic contributions to transport properties based on Maxwell-Stefan theory [93]–[95].
Through the Nernst-Einstein equation, the ionic conductivity can be related to the diffusivity D^{+}, which for monovalent electrolytes (which will be used for demonstrative purposes here) takes the form:

$$\sigma^{+} = \frac{cF}{RT} D^{+},$$

where c is the salt concentration, F is Faraday's constant, R is the gas constant, and T is the temperature. Diffusivities tend to be easier to compute practically when simulating electrolytes, making this a more useful metric. The diffusivity can be approximated through the Stokes-Einstein equation, assuming that the diffusing ion moving amongst solvent molecules can be treated as a macroscopic particle moving through a continuum:

$$D_i = \frac{k_B T}{6\pi\eta r_i},$$

where η is the dynamic viscosity of the electrolyte and r_i is the hydrodynamic radius of species i, typically on the order of $1 < r_i < 10$ Å in typical battery electrolytes [96]. In practice however the diffusion is calculated through a method such as mean squared displacement, or a Green-Kubo equation since the assumptions made for the Stokes-Einstein equation does not hold for all cases, *e.g.* HCEs.

The assumption breaks down for HCEs due to the altered transport mechanism once the amount of salt reaches a certain level. In paper **IV** we show that a percolating network forms, preventing conventional vehicular transport to occur, which is the rule for LE [81], [97]. Instead a process of hopping (also known as a Grotthuss mechanism [98]) is proposed when a proton or positively charged defect, in the case of LIBs this refers to the Li^+ ion, diffuses through a bound network of molecules.[99]. Throughout papers **II-IV** we refer to this mechanism as structural transport, where we include all mass/charge transport that occur through deformations and changes in the macro-molecular structures identified in the electrolyte. The transport mechanisms occurring in LHCEs are still unknown to a large extent, but it is proposed to be a combination between hopping and vehicular transport occur with research being conducted [100]–[102].

From the diffusivity two related, but distinct, and oftentimes confused concepts can be defined: the *transport number*, and the *transference number*. The *transport number* is defined as the fraction of the total current that is carried by the cation, *e.g.* Li^+, assuming no ion aggregation. Conversely the *transference number* is defined as the fraction of the migration current excluding currents due to concentration gradients, that is carried by the cations regardless of the speciation [103]. The migration current is defined as the current driven by an electric field. Under anion blocking conditions, the *transference number* can be described using our previously defined ionic conductivity transport coefficients:

$$t^{\text{abc}}_{\text{trancference}} = \frac{\beta^2 - 4\alpha + 4\alpha^2}{4(1-\alpha)(\beta - 1)}$$

where $\alpha = \frac{\sigma^{++}}{\sigma^{++}+\sigma^{--}}$ reflect the mobility of the cation relative to the anion, and $\beta = \frac{\sigma^{+-}}{\sigma^{++}+\sigma^{--}}$ describes the cation-anion correlation. What can be obtained from MD simulations however is neither of these concepts, but rather t^+, which is oftentimes also called the *transport number* defined as

$$t^+ = \frac{D^+}{D^+ + D^-}.$$

and is identical to the ideal transference number identified by Borodin et al. [104] and very similar to the parameter α we previously defined. Even though the confusion in definitions of transport properties cause problems when comparing studies with each other, concentration trends, *etc.* seem to be consistent enough across methods. In paper **III** we study an array of transport properties using the newly developed CHAMPION software described in paper **II**. This computational method is a simpler way than the experimental methods available to get a measurement of the transference number, where using the Balsara-Newman method [105]:

$$\frac{I_{ss}}{I_0} = \frac{1}{1+Ne} \tag{3.1}$$

$$Ne = a\frac{\sigma RT(1+T_+)^2}{F^2 Dc}\left(1+\frac{d\ln\gamma_+}{d\ln m}\right) \tag{3.2}$$

we have to measure $\frac{I_{ss}}{I_0}$ the steady state current over the initial current, the different parts of the Newman number Ne; the ionic conductivity σ, the diffusion coefficient D, the "thermodynamic factor" $\left(1+\frac{d\ln\gamma_+}{d\ln m}\right)$ to finally be able to calculate the true transference number T_+, whereas computationally we can directly measure the net transfer of a species through CHAMPION.

4

Results & Discussion

In this section the results of the appended papers **I** - **V** are presented and discussed. These move from the molecular level results using DFT methods to determine the Raman spectra of solvation shells (paper **I**), to the microscopic scale where AIMD is used to elucidate what structures form in HCEs (papers **II**,**IV**), and are finally tied together through the use of the newly developed CHAMPION bond graph discovery algorithm (papers **II**, **III**) including a deep dive into the effects of concentration. Finally, a method for enabling large scale simulation with quantum accuracy is suggested using the generalised Åvall method (paper **V**).

4.1 1st Solvation Shells

In order to understand material properties ranging from phase transitions to transport and solvation dynamics it is important to have an understanding of the local environment of a central atom. In paper **I** we wanted to circumvent the usual problems with CaB electrolytes by introducing two, for the chemistry, new electrolyte concepts: HCEs and LHCEs.
The Raman spectra of a wide set of Ca^{2+} 1st solvation shell structures were measured in order to elucidate the local structure within Ca^{2+} HCEs and LHCEs. Artificial Raman spectra are calculated which show that free PC, $[Ca(PC)_4]^{2+}$, free TFSI, and $[Ca(TFSI)_2]$ all play an important role (Fig. 4.1). The remaining structures calculated (Tab. 4.2) show that the PC structures of the form $[Ca((TFSI)_N PC)_M]^{(N-2)-}$ where N is the number of TFSI ions surrounding a central Ca-ion, and M is the number of PC molecules surrounding said Ca ion, where $1 < M < 6$, are almost indistinguishable experimentally.
By the computations in paper **I** the main Raman peaks in the region of interest could be identified. From the combination of experimental Raman data and computational DFT data we could confirm that the first solvation shell is retained when diluting a $Ca(TFSI)_2$:PC HCE with a fluorinated solvent, creating a LHCE. Hence, by understanding the local structure we can make better predictions when searching for, in this case, CaB-electrolytes that have the potential for SEI formation, meaning they are more likely to cycle stably at room temperature.
Generalising from paper **I** and similar studies done in literature [106]–[108] we see that by understanding the local structure the design of electrolytes can be aided. DFT works well as a complementary method to Raman spectroscopy, amongst many other experimental methods. However, even if DFT is a capable descriptive method, in order to make predictions about structure ,DFT is not the most optimal method.

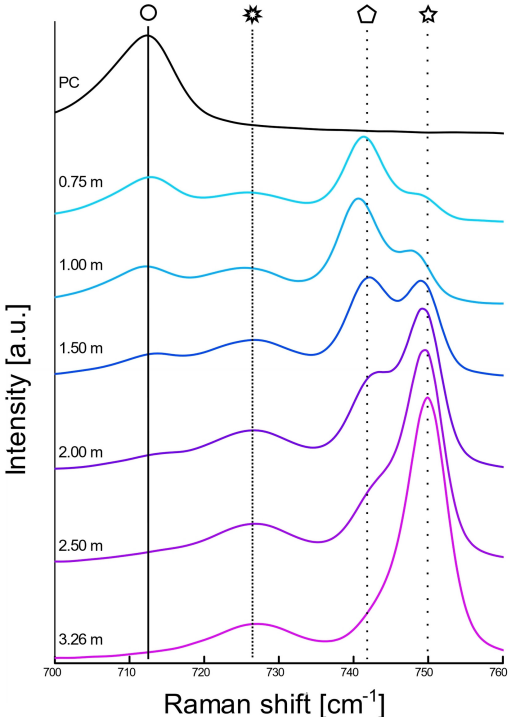

(a) Band assignments of HCE and LE through the use of DFT (symbol key subFig. 4.1c).

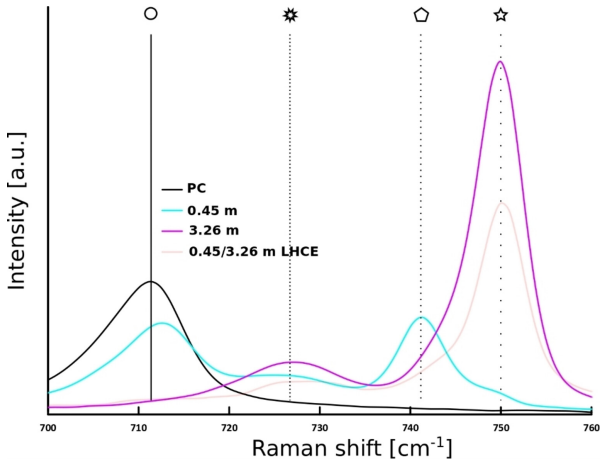

(b) Band assignment when diluting HCE from 3.256 m to a nominal 0.45 m LHCE (symbol key subFig. 4.1c).

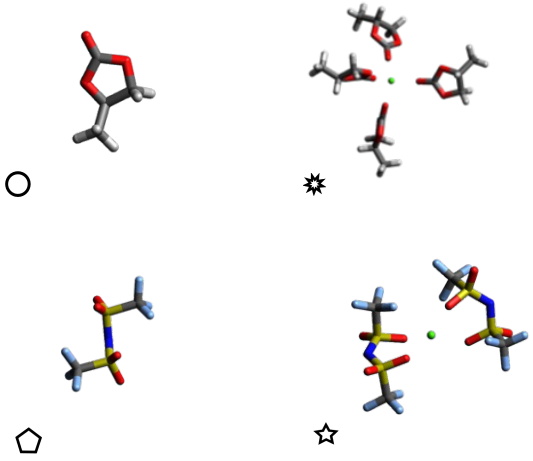

(c) A symbol key to 4.1a and 4.1b . Free PC (○), $[Ca(PC)_4]^{2+}$ (✹), free TFSI (⬠), $[Ca(TFSI)_2]$ (☆).

Figure 4.1: Use of DFT to elucidate the local bulk structure in electrolytes.

Table 4.2: Comparison between selected experimental and computational DFT Raman data. $\bar{x}$ denotes the average Raman activity of the species.

	Computational		Experimental
Species	Frequency [cm^{-1}]	Raman Activity [$Å^4 amu^{-1}$]	Raman shift [cm^{-1}]
PC	715	6.1	713
$[Ca(PC)]^{2+}$	735	7.1	721, 728, 734
$[Ca(PC)_4]^{2+}$	738	12	
	738	10	
	739	15	
	742	15 $\bar{x} = 13$	
$[Ca(PC)_5]^{2+}$	736	22	
	737	0.16	
	739	15	
	739	8.3	
	743	17 $\bar{x} = 12$	
$[Ca(PC)_6]^{2+}$	732	21	
	732	19	
	733	0.52	
	733	0.21	
	734	1.9	
	737	22 $\bar{x} = 11$	
$[TFSI]^-$ (C_1)	755	2.8	741
$[TFSI]^-$ (C_2)	755	2.8	
$Ca[TFSI]_2$ (C_1)	771	3.1	750
	787	3.9	
$Ca[TFSI]_2$ (C_2)	775	2.4	
	778	10	
$Ca[TFSI]_2$ (D_2)	770	1.1	
	771	5.3	

Convention dictates that DFT structures are set up by a researcher according to what is deemed feasible, with great success might add. However there are stark limitations, mainly from said researchers imagination. We see in papers **III** and **IV** many non-trivial structures can form (Fig 4.3, Fig 4.10), especially when looking beyond the first solvation shell.
Hence, to enable large electrolyte screenings, one possible venue is to combine these methods in the future. The local structures obtained from CHAMPION analyses of MD data is great input to DFT simulations, and it provides a more replicable representation of possible structures than an individual researchers intuition.

4.2 From Local to Global Structure

In paper **II**, **III** **IV** we identify how to use the newly developed CHAMPION method together with AIMD simulations to gain knowledge of both the local and global

electrolyte structure. AIMD enables simulations where the local interactions are replicated accurately, as can be observed with the coordination number (CN) for $Li^+ \approx 4$, which is common for LIB electrolytes based on small organic molecules, regardless of composition [109], [110]. In many electrolytes CN is similar to the solvation number (SN) since almost all coordinations are monodentate. This is, however, not true for LiTFSI in ACN at higher concentrations where the SN is closer to 3, even though the CN remains close to 4 due to more bidentate TFSI coordination by Li^+, which concurs with other studies [111]. These results from paper **III**, studying LiTFSI:2ACN, are reflected in the common topologies (Fig. 4.3) found in the simulation.

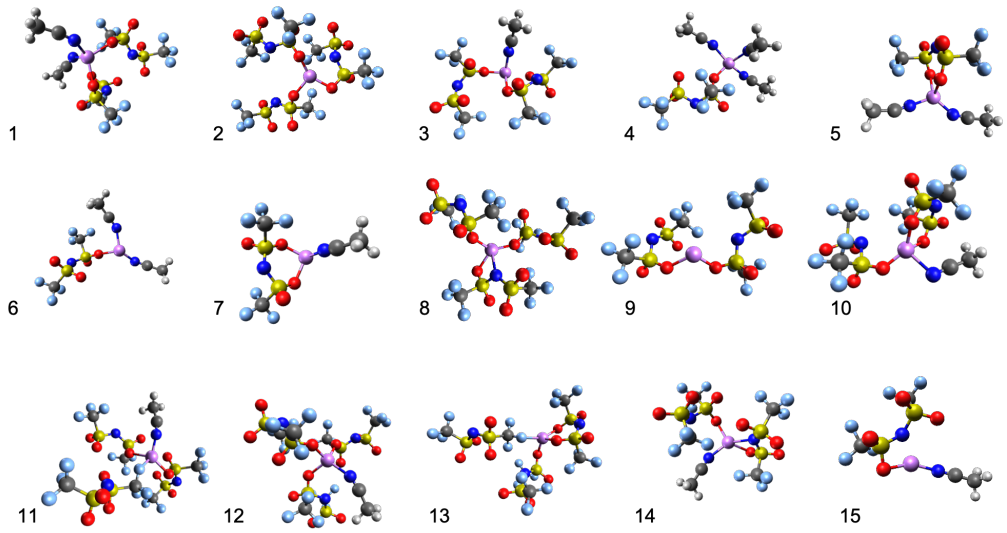

Figure 4.3: The most common topologies around a Li cation in order of probability. Element colors: purple: Li, red: O, blue: N, grey: C, white: H, yellow: S, green: F.

On a global scale we see that these structures form a percolating network, in a sea of free solvent (Fig. 4.4), which is in sharp contrast to the common conception about HCEs, where its unique behaviour is believed to stem from a lack of free solvent [99]. This view is also supported by the distribution of the number of ligands surrounding both cation and anion (Fig 4.5). We see that a majority of TFSI-ions are coordinated to two or more Li^+, and focusing on the Li^+-ion we similarly see that a majority of these are also coordinated to two or more TFSI-ions, which can only occur if all ions are part of one large, global structure.
The accuracy of this analysis scales with the number of ions and even for a concentrated system such as this, system size and trajectory length are both on the smaller scale in order to say something with statistical accuracy. Hence less concentrated systems, such as LHCEs for example, require much larger simulations to enable the same accuracy level as the analysis results of a HCE which more or less disqualify AIMD for such systems.

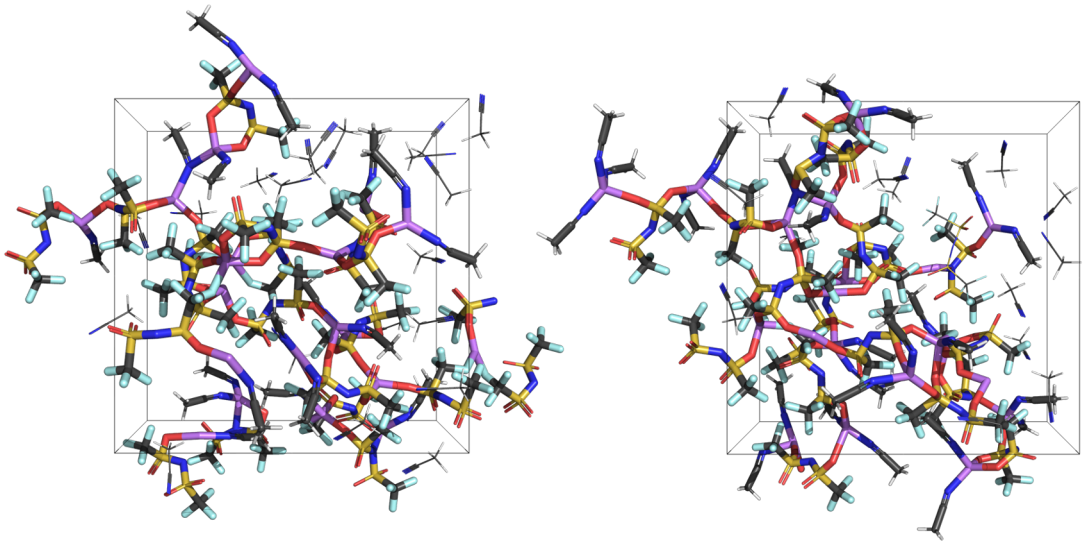

Figure 4.4: Snapshots of the periodic simulation cell, highlighting the percolating network in a sea of solvent.

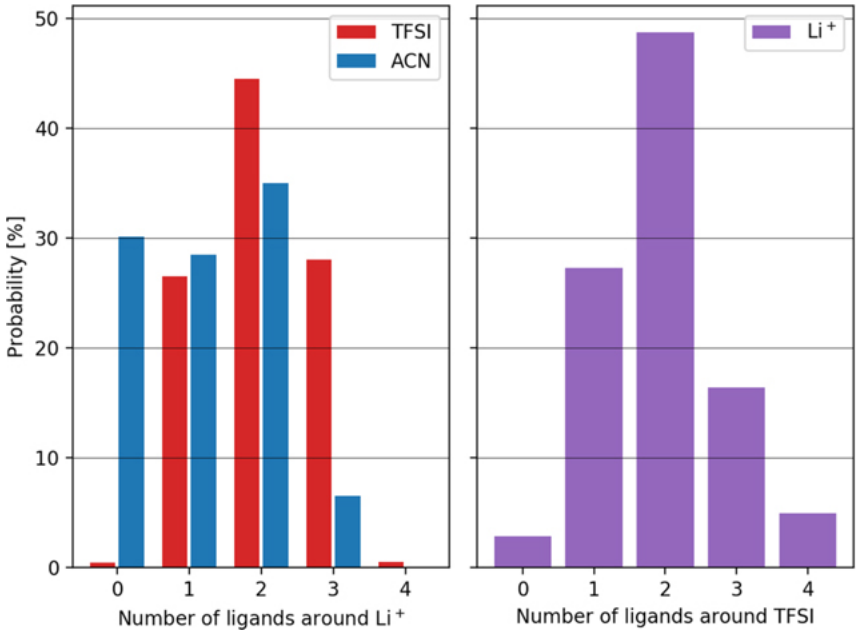

Figure 4.5: Distribution of (left) TFSI ions and ACN molecules coordinating to Li^+ and (right) Li^+ ions coordinating to TFSI.

4.3 Role(s) of Salt Concentration

Extending on the structural analysis carried out in paper **III**, we showcase the true strength of the CHAMPION software in paper **IV** by performing a screening study of several similar systems. We are directly able to describe the emergence of HCE behaviour by investigating the structural changes when increasing the salt concentration of LiTFSI:ACN from 1:16, 1:9, 1:4, to 1:2. Similarly to the behaviour we saw in paper **III** the percolating network is apparent in the 1:2 system in paper

IV, note that the behaviour is more extreme in this paper due to studying a more equilibrated system (Fig 4.6). Comparing with experimental data performed by Seo et al. [111] we see that the results obtained through our CHAMPION analysis of data computed using PBE coincides well (Fig 4.7).

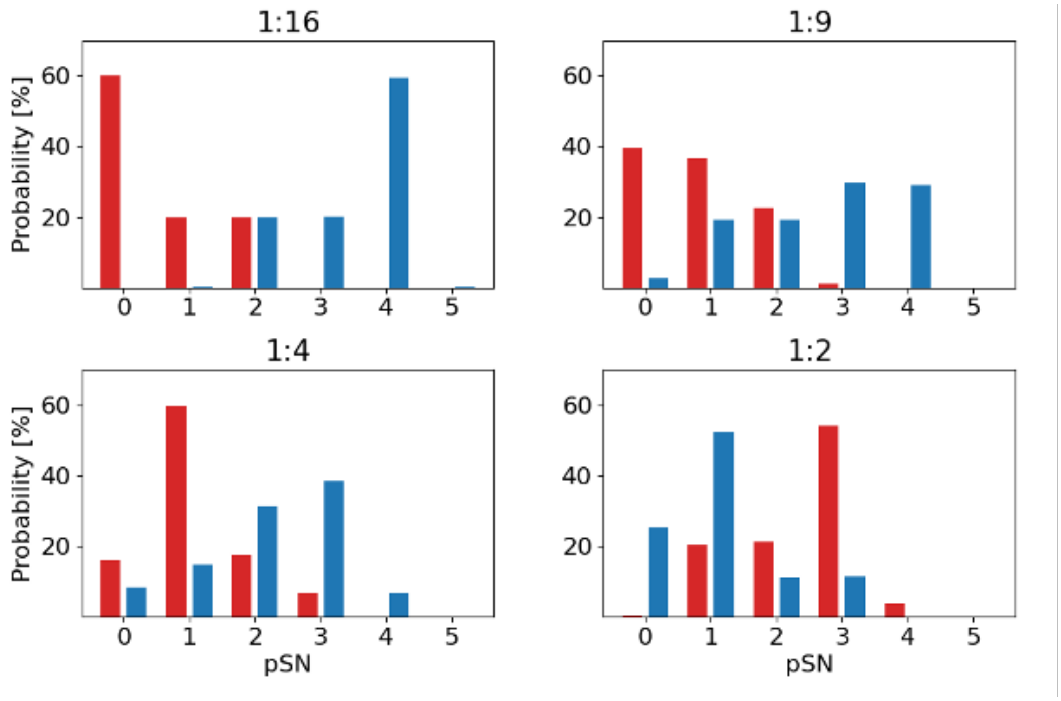

Figure 4.6: pSN_{ACN} (blue) and pSN_{TFSI} (red) for the four electrolytes in paper **IV**.

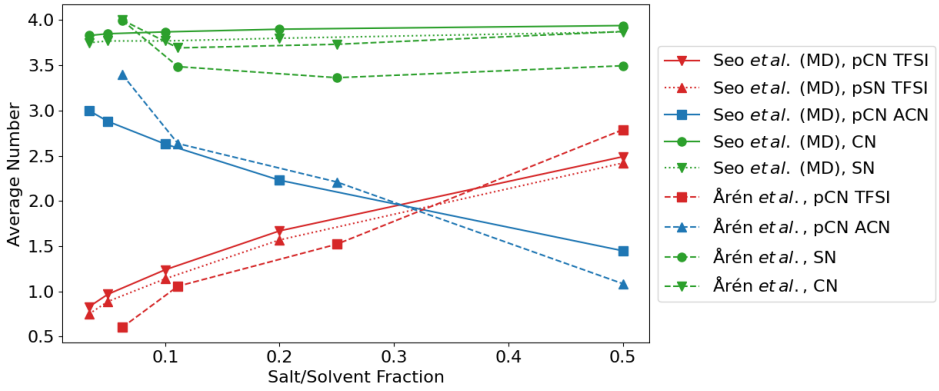

Figure 4.7: (p)CNs and (p)SNs, comparing our data with Seo et al.

Looking at the average and maximum aggregate size as well as the free fraction of solvent and anion (Fig 4.8) we were able to show a clear trend towards forming a large network structure at high concentrations. Also this agree well with literature [111], [112] (Fig. 4.9). We stress that unlike conventional knowledge, which argue that lack of free solvent being a key feature of HCEs, we show that even for the most

extreme HCE a substantial amount of solvent remains free, an insight only made possible by our deeper understanding of the electrolyte structure.

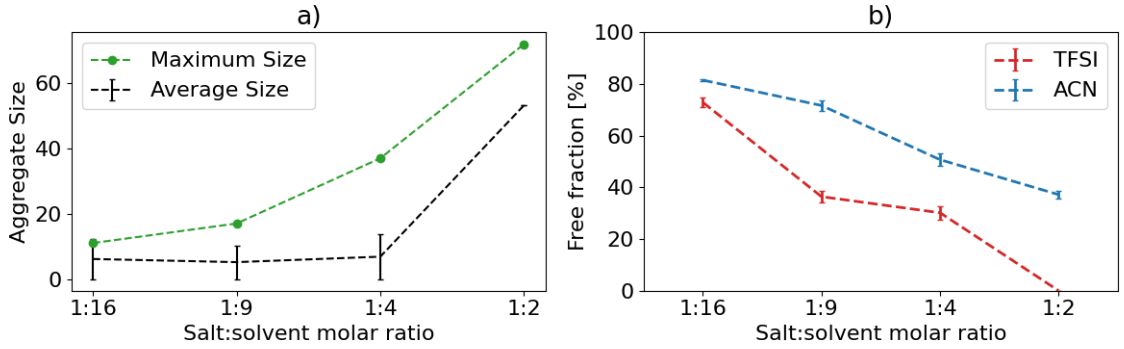

Figure 4.8: a) Average and maximum aggregate size in number of total ions and solvent molecules in connected components, and b) fraction of free, i.e. uncoordinated to Li^+, anions and solvent molecules, as functions of electrolyte salt concentration. (For 1:2 too few data points become available to make an error-bar sensible in a).)

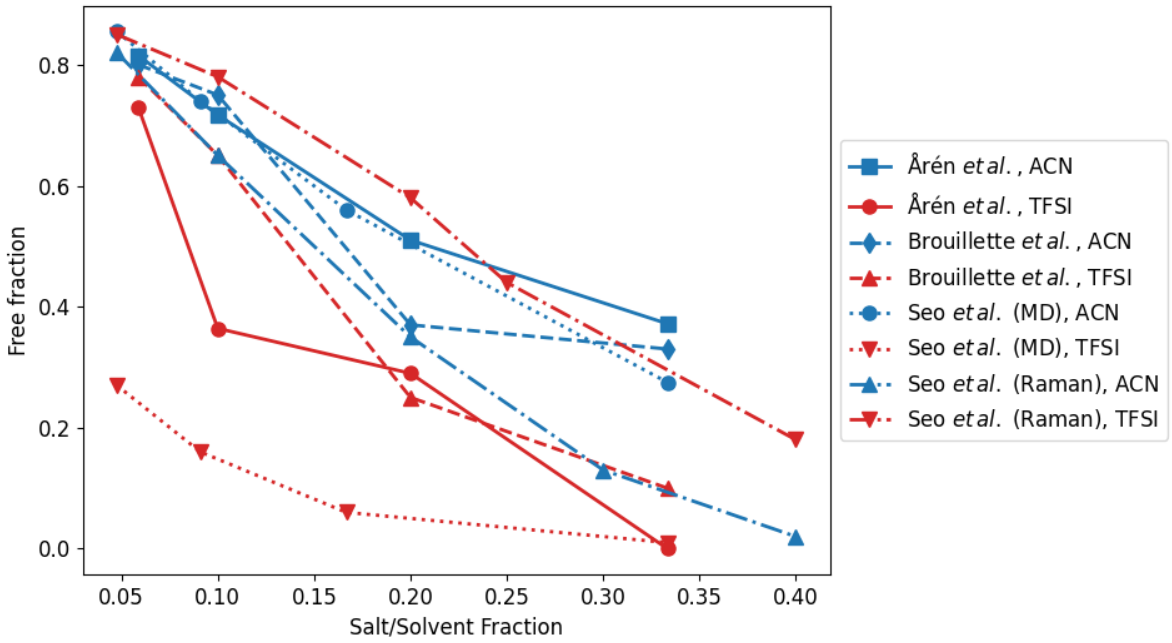

Figure 4.9: Fraction of free ACN and TFSI as function of LiTFSI molar fraction, comparing our data with available data from literature.

Similarly the type of structure analysis CHAMPION enables gives a deeper understanding in how the species distribution change as a function of concentration (Fig 4.10). A clear picture emerges of how the local environment around lithium becomes more complex the more salt is added, with the 1:16 LiTFSI:ACN system being fully made up by the top five species, whilst in the 1:2 system less than 70% of the lithium resides in the top five.

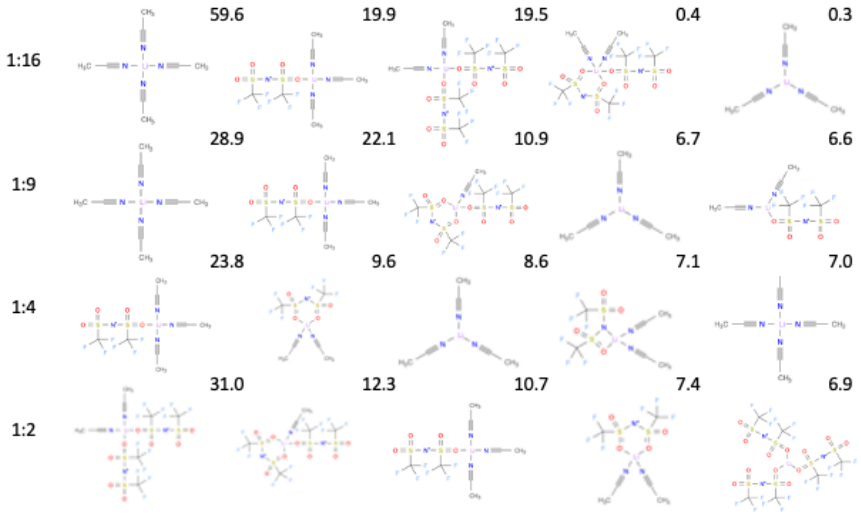

Figure 4.10: The topologies and percentage fraction of the five most common local structures for the four electrolytes.

Somewhat counter-intuitive given the previous insight, but still consistent with literature [113], [114] the configurational entropy of LiTFSI in ACN decreases (Fig 4.11) as concentration rises. Even though local complexity rises, the global structure gets more ordered, forming one big structure (Fig 4.8 a)), a percolating network.

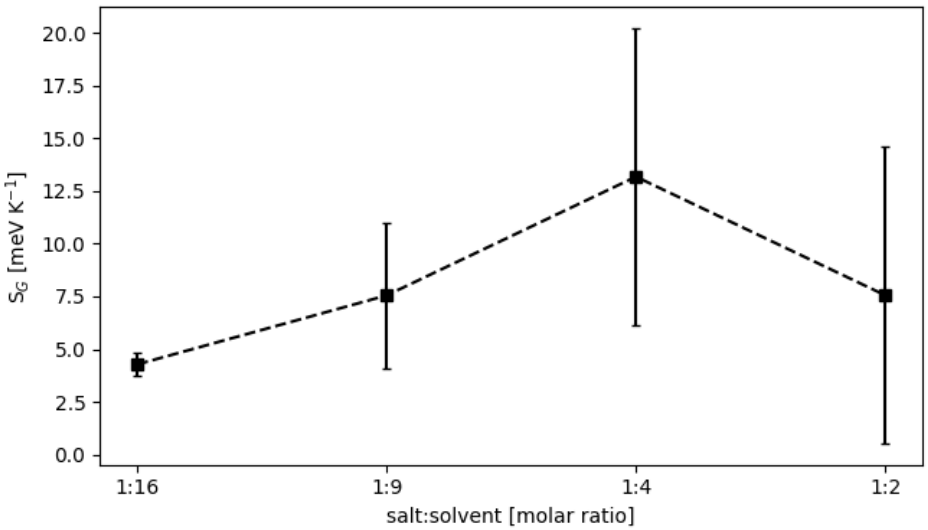

Figure 4.11: Configurational entropy as a function of electrolyte salt concentration.

However, to make full use of these types of analysis, we would ideally like to probe further along the temporal dimension, as well as have better statistics from a larger sample. The method used to evaluate the forces, CPMD with the PBE functional, generalise well to a wide array of systems, but AIMD still heavily impact computational resources, making it non-viable for more exhaustive studies.

4.4 The Dream of a Force Field to Rule Them All

As mentioned above large scale simulations must be utilised to make full use of computational material science in general and the CHAMPION method in particular. The systems that would benefit the most from this (HCEs, LHCEs, ionic liquids *etc.*) employ FFs that usually do not capture the correct dynamics [14]. In this context, paper **V** focuses on extending the functionality of CHAMPION by combining it with the insights gained in Åvall & Johansson 2020 [20].
As a proof of concept the method was applied to the simplest case possible: a noble gas modelled using a LJ potential and fit the raw data to a curve using a kernel smoother.
The obtained $r^2 = 0.923$ (Fig 4.12) indicates that capture some of the dynamics, but not yet at accuracy on par with conventional NN methods. Comparing with Hellström and Behler's [115] NN study of aqueous electrolytes with a root mean squared error (RMSE), = 0.28 nN, our RMSE = 2.55 nN. Using the theoretical LJ force curve, however, our RMSE = 0.28 nN.

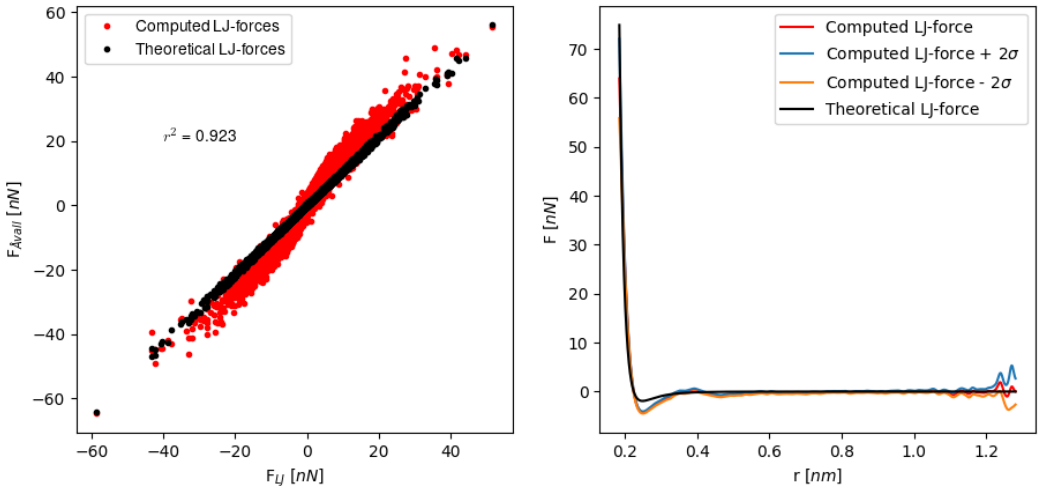

Figure 4.12: a) Force-force scatter plot using both the computed and theoretical LJ potential derivative to evaluate forces. r^2 calculated for the computed LJ-forces. b) Computed and theoretical LJ potential derivative.

The remaider of paper **V** is still under development, where the full set of interaction curves described by the *natural internal coordinates* for LiTFSI:ACN 1:9 is being produced.

5
Conclusion & Outlook

This thesis has studied battery electrolytes using computational means at different scales, and made suggestions for a work flow in order to better combine the strength of each of the methods used at the different scales. Starting with paper **I** studying the local structure of electrolytes using DFT, and aiding in showing that the local structure of HCEs are retained in LHCEs. From this we are able to create hypotheses regarding macroscopic properties. In paper **II** we create a new method of detecting structure in materials simulations, especially in liquids, which is used to aid us describe the structural and transport behaviour we observe in papers **III** and **IV**, enabling us to gain completely new insights into what might be the defining quality of HCEs. Through understanding how the local structure gives rise to the global structure, and how the global structure can be used to explain transport properties, these two papers exemplify how computational methods open up a future where materials science can be made more effective and predictive, especially building upon the screening in paper **IV** with substantial gains in understanding to be had pre-screening large amounts of materials. Especially if this methodology is combined with experimental design schemes such as e.g. design of experiment (DOE) [116], [117].

In order to enable such screenings to be viable, large scale MD simulations have to be easily available. In paper **V** the development of a method trying to tackle this problem was initiated, however much work is still needed on this method, mainly on optimising the curve fitting algorithm as to obtain a closer fit to the ideal curve. If successful this could open up for order of magnitude faster materials computations; evaluating the xTB forces used in paper **V** took 208 core hours at a modern supercomputer (vera@c3se), whilst evaluating the same forces using the Åvall method took less than a minute using a single thread on a standard laptop computer. In paper **V** we propose the following actions as a way forward in developing the Åvall method:

- Optimize model parameters to better match force curves.
- Create a MD solver specialized in using this type of new FF.
- Showcase a better fit to theoretical forces.

Given all these pieces it would be interesting to study large scale simulations of LHCEs and studying how these systems behave and what structures form on a global scale. Especially the cumulative effects when large scale MD simulations for any material quickly and cost effectively is combined with the CHAMPION

analysis. Through such endeavours it will be most interesting, seeing what physical properties can be explained this way. These types of studies should enable probing the phase separation between the diluent and the HCE structures, making it possible to study cluster formation, and cluster size, transport phenomena *etc.* Similarly the combination of the methods presented in this thesis could provide an avenue to study electrolyte-electrode interface and interphase interactions. From there on it is up to the imagination of the reader to find interesting problems where these methods can be applied.

Acknowledgements

I would like to start by thanking my supervisor Professor Patrik Johansson for giving me the freedom to pursue research unconstrained, and for all the support in writing this thesis. Secondly Professor Aleksandar Matic, my examiner and closest boss, thank you for keeping spirits up around (K)MF both online and offline during my almost 6 year long stay. Thank you Dr. Rasmus Andersson for your continuous support, friendship, and rubber ducking. Without the discussions you and I have had throughout the years we would not be where we are now. I am looking forward to continue to revolutionise materials development togheter with you. I would also like to thank all the colleagues at (K)MF that have come and gone throughout the years, you make the PhD candidate life easier and I want to give an extra shout out to my co-authors both at the department such as Pierre, and Gustav and abroad, like Alejandro, Chris, and many others. In addition I would like to send a big thank you to Victor Westergård and Peter Deaking and the Chalmers Innovation office for all help with patenting our insights. I would like to thank Emil Krutmeijer, Johannes Henriksson, and Rasmus yet again, my teammates at Compular, the ball is rolling let's keep it up! Also thanks to Magnus, Laetitia, Per, Robert, and Romina, it feels amazing to know you are joining in the vision to digitalize materials development! Thank you to my mother Agneta and father Mille for supporting me throughout my life. I would also like to show my appreciation to my funders, the HELIS project (European Union's Horizon 2020 research and innovation program under Grant Agreement No. 666221), Horizon 2020 research and innovation programme H2020 FETOPEN-1-2016-2017 (CARBAT grant agreement #766617), the Swedish Energy Agency grants (#P43525-1 and #P39909-1), and the Chalmers Areas of Advance: Materials Science, Energy, and Transport for enabling it all as well as the Swedish National Infrastructure for Computing (SNIC) for providing my work with computational resources. I would also like to acknowledge several of Chalmers Areas of Advance: Materials Science, Energy, and Transport, for continuous support.
Lastly I would like to thank you the reader for taking the time to read this thesis!

Fabian Årén, Gothenburg, May 2023

Bibliography

[1] M. McLuhan, W. T. Gordon, E. Lamberti, and D. Scheffel-Dunand, *The Gutenberg galaxy: The making of typographic man*. University of Toronto Press, 2011.

[2] R. W. Emerson, *Society and solitude. Twelve chapters.* Boston: Fields, Osgood & Co., 1870.

[3] W. D. Henry Ward Beecher, *Proverbs from Plymouth pulpit;* New York: D. Appleton and Co., 1887.

[4] J. McMahon, *Why Energy Storage Is Proving Even More Disruptive Than Cheap Renewables*, https://www.forbes.com/sites/jeffmcmahon/2019/08/02/why-energy-storage-is-proving-even-more-disruptive-than-cheap-renewables/, Section: Sustainability.

[5] G. E. Blomgren, "The Development and Future of Lithium Ion Batteries," *J. Electrochem. Soc.*, vol. 164, no. 1, A5019–A5025, Jan. 2017, Number: 1 Reporter: J. Electrochem. Soc.

[6] N. Kuchai, P. Shepherd, J. Calabria-Holley, A. Copping, A. Matard, and D. Coley, "The potential for computational IT tools in disaster relief and shelter design," *Journal of International Humanitarian Action*, vol. 5, no. 1, p. 1, Apr. 2020.

[7] A. Mongia, S. K. Saha, E. Chouzenoux, and A. Majumdar, "A computational approach to aid clinicians in selecting anti-viral drugs for COVID-19 trials," *Scientific Reports*, vol. 11, no. 1, p. 9047, Apr. 2021, Number: 1 Publisher: Nature Publishing Group.

[8] P. A. M. Dirac, "Quantum mechanics of many-electron systems," *Proceedings of the Royal Society of London. Series A, Containing Papers of a Mathematical and Physical Character*, vol. 123, no. 792, pp. 714–733, 1929.

[9] *The Nobel Prize in Chemistry 1998*, https://www.nobelprize.org/prizes/chemistry/1998/8811-the-nobel-prize-in-chemistry-1998/, 2021-06-21.

[10] B. J. Alder and T. E. Wainwright, "Studies in molecular dynamics. i. general method," *The Journal of Chemical Physics*, vol. 31, no. 2, pp. 459–466, 1959. eprint: `https://doi.org/10.1063/1.1730376`.

[11] J. B. Gibson, A. N. Goland, M. Milgram, and G. H. Vineyard, "Dynamics of radiation damage," *Phys. Rev.*, vol. 120, pp. 1229–1253, 4 Nov. 1960.

[12] *The Nobel Prize in Chemistry 2013*, https://www.nobelprize.org/prizes/chemistry/2013/summary/, 2021-05-31.

[13] S.-P. Kim, A. C. T. v. Duin, and V. B. Shenoy, "Effect of electrolytes on the structure and evolution of the solid electrolyte interphase (SEI) in Li-ion batteries: A molecular dynamics study," *Journal of Power Sources*, vol. 196, no. 20, pp. 8590–8597, 2011.

[14] D. Bedrov, J.-P. Piquemal, O. Borodin, A. D. MacKerell Jr, B. Roux, and C. Schröer, "Molecular dynamics simulations of ionic liquids and electrolytes using polarizable force fields," *Chemical Reviews*, vol. 119, no. 13, pp. 7940–7995, 2019.

[15] B. Ravikumar, M. Mynam, and B. Rai, "Effect of salt concentration on properties of lithium ion battery electrolytes: A molecular dynamics study," *The Journal of Physical Chemistry C*, vol. 122, no. 15, pp. 8173–8181, 2018.

[16] P. Yoo, M. Sakano, S. Desai, M. M. Islam, P. Liao, and A. Strachan, "Neural network reactive force field for C, H, N, and O systems," *npj Computational Materials*, vol. 7, no. 1, pp. 1–10, 2021.

[17] J. S. Smith, O. Isayev, and A. E. Roitberg, "ANI-1: an extensible neural network potential with DFT accuracy at force field computational cost," *Chemical Science*, vol. 8, no. 4, pp. 3192–3203, 2017.

[18] H.-X. Li, X.-Y. Zhou, Y.-C. Wang, and H. Jiang, "Theoretical study of Na^+ transport in the solid-state electrolyte Na_3OBr based on deep potential molecular dynamics," *Inorganic Chemistry Frontiers*, vol. 8, no. 2, pp. 425–432, 2021.

[19] D. Castelvecchi, "Can we open the black box of AI?" *Nature News*, vol. 538, no. 7623, p. 20, 2016.

[20] G. Åvall and P. Johansson, "A novel approach to ligand-exchange rates applied to lithium-ion battery and sodium-ion battery electrolytes," *The Journal of Chemical Physics*, vol. 152, no. 23, p. 234 104, 2020.

[21] E. Weinan, *Principles of multiscale modeling*. Cambridge University Press, 2011.

[22] *Citation report DFT batteries 2023*, https://www.webofscience.com/wos/woscc/citation-report/d2f58c33-cf9a-4f49-8a12-4cdc305256c7-6bc59d5f?sort=date-ascending&page=1, 2023-01-23.

[23] M. A. Nielsen and I. Chuang, *Quantum computation and quantum information*. American Association of Physics Teachers, 2002.

[24] J. Thijssen, *Computational physics*, Second. Cambridge university press, 2007.

[25] Y. Zhao and D. G. Truhlar, "The M06 suite of density functionals for main group thermochemistry, thermochemical kinetics, noncovalent interactions, excited states, and transition elements: Two new functionals and systematic testing of four M06-class functionals and 12 other functionals," *Theoretical Chemistry Accounts*, vol. 120, no. 1, pp. 215–241, May 2008.

[26] K. Kim and K. D. Jordan, "Comparison of Density Functional and MP2 Calculations on the Water Monomer and Dimer," *The Journal of Physical Chemistry*, vol. 98, no. 40, pp. 10 089–10 094, Oct. 1994, Publisher: American Chemical Society.

[27] J. P. Perdew, K. Burke, and M. Ernzerhof, "Generalized gradient approximation made simple," *Physical Review Letters*, vol. 77, no. 18, p. 3865, 1996.

[28] *Citation report molecular dynamics batteries 2023*, 2023-01-23.

[29] D. A. Case, T. E. Cheatham III, T. Darden, H. Gohlke, R. Luo, K. M. Merz Jr, A. Onufriev, C. Simmerling, B. Wang, and R. J. Woods, "The Amber biomolecular simulation programs," *Journal of Computational Chemistry*, vol. 26, no. 16, pp. 1668–1688, 2005.

[30] B. R. Brooks, C. L. Brooks III, A. D. Mackerell Jr, L. Nilsson, R. J. Petrella, B. Roux, Y. Won, G. Archontis, C. Bartels, S. Boresch, *et al.*, "CHARMM: The biomolecular simulation program," *Journal of Computational Chemistry*, vol. 30, no. 10, pp. 1545–1614, 2009.

[31] M. J. Abraham, T. Murtola, R. Schulz, S. Páll, J. C. Smith, B. Hess, and E. Lindahl, "GROMACS: High performance molecular simulations through multi-level parallelism from laptops to supercomputers," *SoftwareX*, vol. 1, pp. 19–25, 2015.

[32] A. C. Van Duin, S. Dasgupta, F. Lorant, and W. A. Goddard, "Reaxff: A reactive force field for hydrocarbons," *The Journal of Physical Chemistry A*, vol. 105, no. 41, pp. 9396–9409, 2001.

[33] M. J. Hossain, G. Pawar, B. Liaw, K. L. Gering, E. J. Dufek, and A. C. Van Duin, "Lithium-electrolyte solvation and reaction in the electrolyte of a lithium ion battery: A reaxff reactive force field study," *The Journal of Chemical Physics*, vol. 152, no. 18, p. 184 301, 2020.

[34] G. Shchygol, A. Yakovlev, T. Trnka, A. C. T. van Duin, and T. Verstraelen, "ReaxFF Parameter Optimization with Monte-Carlo and Evolutionary Algorithms: Guidelines and Insights," *Journal of Chemical Theory and Computation*, vol. 15, no. 12, pp. 6799–6812, Dec. 2019, Publisher: American Chemical Society.

[35] R. Car and M. Parrinello, "Unified approach for molecular dynamics and density-functional theory," *Physical Review Letters*, vol. 55, no. 22, p. 2471, 1985.

[36] M. Elstner and G. Seifert, "Density functional tight binding," *Philosophical Transactions of the Royal Society A: Mathematical, Physical and Engineering Sciences*, vol. 372, no. 2011, p. 20 120 483, 2014.

[37] C. Bannwarth, E. Caldeweyher, S. Ehlert, A. Hansen, P. Pracht, J. Seibert, S. Spicher, and S. Grimme, "Extended tight-binding quantum chemistry methods," *Wiley Interdisciplinary Reviews: Computational Molecular Science*, vol. 11, no. 2, e1493, 2021.

[38] J. VandeVondele, M. Krack, F. Mohamed, M. Parrinello, T. Chassaing, and J. Hutter, "Quickstep: Fast and accurate density functional calculations using a mixed gaussian and plane waves approach," *Computer Physics Communications*, vol. 167, no. 2, pp. 103–128, 2005.

[39] J. Hutter and M. Iannuzzi, "CPMD: Car-parrinello molecular dynamics," *Zeitschrift für Kristallographie-Crystalline Materials*, vol. 220, no. 5-6, pp. 549–551, 2005.

[40] S. A. Hollingsworth and R. O. Dror, "Molecular dynamics simulation for all," *Neuron*, vol. 99, no. 6, pp. 1129–1143, 2018.

[41] R. ANDERSSON, F. ÅRÉN, and P. JOHANSSON, *Method and device for determining bonds in particle trajectories*, SE 2051245-5.

[42] V. Bonnici, R. Giugno, A. Pulvirenti, D. Shasha, and A. Ferro, "A subgraph isomorphism algorithm and its application to biochemical data," *BMC bioinformatics*, vol. 14, no. 7, pp. 1–13, 2013.

[43] J. Behler and M. Parrinello, "Generalized neural-network representation of high-dimensional potential-energy surfaces," *Physical Review Letters*, vol. 98, no. 14, p. 146 401, 2007.

[44] A. P. Bartók, M. C. Payne, R. Kondor, and G. Csányi, "Gaussian approximation potentials: The accuracy of quantum mechanics, without the electrons," *Physical Review Letters*, vol. 104, no. 13, p. 136 403, 2010.

[45] A. P. Bartók, R. Kondor, and G. Csányi, "On representing chemical environments," *Physical Review B*, vol. 87, no. 18, p. 184 115, 2013.

[46] K. T. Schütt, H. E. Sauceda, P.-J. Kindermans, A. Tkatchenko, and K.-R. Müller, "Schnet–a deep learning architecture for molecules and materials," *The Journal of Chemical Physics*, vol. 148, no. 24, p. 241 722, 2018.

[47] W. Wang, T. Yang, W. H. Harris, and R. Gómez-Bombarelli, "Active learning and neural network potentials accelerate molecular screening of ether-based solvate ionic liquids," *Chemical Communications*, vol. 56, no. 63, pp. 8920–8923, 2020.

[48] P. Meltzer, M. D. G. Mallea, and P. J. Bentley, "Pinet: A permutation invariant graph neural network for graph classification," *arXiv preprint arXiv:1905.03046*, 2019.

[49] L. Knijff and C. Zhang, "Machine learning inference of molecular dipole moment in liquid water," *arXiv preprint arXiv:2103.08274*, 2021.

[50] S. Dajnowicz, G. Agarwal, J. M. Stevenson, L. D. Jacobson, F. Ramezanghorbani, K. Leswing, R. A. Friesner, M. D. Halls, and R. Abel, "High-dimensional neural network potential for liquid electrolyte simulations," *The Journal of Physical Chemistry B*, vol. 126, no. 33, pp. 6271–6280, 2022.

[51] J. Zhang, J. Pagotto, and T. T. Duignan, "Towards predictive design of electrolyte solutions by accelerating ab initio simulation with neural networks," *Journal of Materials Chemistry A*, vol. 10, no. 37, pp. 19 560–19 571, 2022.

[52] E. Kocer, J. K. Mason, and H. Erturk, "A novel approach to describe chemical environments in high-dimensional neural network potentials," *The Journal of Chemical Physics*, vol. 150, no. 15, p. 154 102, 2019.

[53] *BIG-MAP*, https://www.big-map.eu/big-map, 2021-05-30.

[54] *Materials Genome Initiative | WWW.MGI.GOV*, https://www.mgi.gov/, 2021-05-30.

[55] W. Wang, Z. Wu, J. C. Dietschreit, and R. Gómez-Bombarelli, "Learning pair potentials using differentiable simulations," *The Journal of Chemical Physics*, vol. 158, no. 4, p. 044 113, 2023.

[56] A. S. Fraser, "Simulation of genetic systems by automatic digital computers i. introduction," *Australian Journal of Biological Sciences*, vol. 10, no. 4, pp. 484–491, 1957.

[57] E. Zitzler and L. Thiele, "Multiobjective evolutionary algorithms: A comparative case study and the strength pareto approach," *IEEE transactions on Evolutionary Computation*, vol. 3, no. 4, pp. 257–271, 1999.

[58] W. M. Spears, *Evolutionary Algorithms: the role of mutation and recombination*. Springer Science & Business Media, 2013.

[59] F. Pedregosa, G. Varoquaux, A. Gramfort, V. Michel, B. Thirion, O. Grisel, M. Blondel, P. Prettenhofer, R. Weiss, V. Dubourg, J. Vanderplas, A. Passos, D. Cournapeau, M. Brucher, M. Perrot, and E. Duchesnay, "Scikit-learn: Machine learning in Python," *Journal of Machine Learning Research*, vol. 12, pp. 2825–2830, 2011.

[60] D. Duvenaud, "Automatic model construction with gaussian processes," Ph.D. dissertation, University of Cambridge, 2014.

[61] F. Årén, *Machine learning force fields for highly concentrated electrolytes*, Master Thesis, 2018, University of Gothenburg, Department of Physics.

[62] J. Zwicker and R. Lovett, "When does a pair correlation function fix the state of an equilibrium system?" *The Journal of Chemical Physics*, vol. 93, no. 9, pp. 6752–6755, 1990.

[63] V. Bakken and T. Helgaker, "The efficient optimization of molecular geometries using redundant internal coordinates," *The Journal of Chemical Physics*, vol. 117, no. 20, pp. 9160–9174, 2002.

[64] J. B. Goodenough and Y. Kim, "Challenges for rechargeable Li batteries," *Chemistry of Materials*, vol. 22, no. 3, pp. 587–603, 2010.

[65] Y. Wu, *Lithium-ion batteries: Fundamentals and Applications*. CRC press, 2015, vol. 4.

[66] C. Arbizzani, G. Gabrielli, and M. Mastragostino, "Thermal stability and flammability of electrolytes for lithium-ion batteries," *Journal of Power Sources*, vol. 196, no. 10, pp. 4801–4805, 2011.

[67] G. G. Botte, R. E. White, and Z. Zhang, "Thermal stability of LiPF6–EC: EMC electrolyte for lithium ion batteries," *Journal of Power Sources*, vol. 97, pp. 570–575, 2001.

[68] T. Kawamura, A. Kimura, M. Egashira, S. Okada, and J.-I. Yamaki, "Thermal stability of alkyl carbonate mixed-solvent electrolytes for lithium ion cells," *Journal of Power Sources*, vol. 104, no. 2, pp. 260–264, 2002.

[69] Z. Yu, T. R. Juran, X. Liu, K. S. Han, H. Wang, K. T. Mueller, L. Ma, K. Xu, T. Li, L. A. Curtiss, *et al.*, "Solvation structure and dynamics of $Mg(TFSI)_2$ aqueous electrolyte," *Energy & Environmental Materials*, vol. 5, no. 1, pp. 295–304, 2022.

[70] F. Lundin, L. Aguilera, H. W. Hansen, S. Lages, A. Labrador, K. Niss, B. Frick, and A. Matic, "Structure and dynamics of highly concentrated LiTFSI/acetonitrile electrolytes," *Physical Chemistry Chemical Physics*, vol. 23, no. 25, pp. 13 819–13 826, 2021.

[71] A. Ponrouch, C. Frontera, F. Bardé, and M. R. Palacıén, "Towards a calcium-based rechargeable battery," *Nature Materials*, vol. 15, no. 2, pp. 169–172, 2016.

[72] D. Wang, X. Gao, Y. Chen, L. Jin, C. Kuss, and P. G. Bruce, "Plating and stripping calcium in an organic electrolyte," *Nature Materials*, vol. 17, no. 1, pp. 16–20, 2018.

[73] G. Jiang, F. Li, H. Wang, M. Wu, S. Qi, X. Liu, S. Yang, and J. Ma, "Perspective on High-Concentration Electrolytes for Lithium Metal Batteries," *Small Structures*, p. 2 000 122, 2021.

[74] Y. Yamada, K. Furukawa, K. Sodeyama, K. Kikuchi, M. Yaegashi, Y. Tateyama, and A. Yamada, "Unusual stability of acetonitrile-based superconcentrated electrolytes for fast-charging lithium-ion batteries," *Journal of the American Chemical Society*, vol. 136, no. 13, pp. 5039–5046, 2014.

[75] R. Petibon, C. Aiken, L. Ma, D. Xiong, and J. Dahn, "The use of ethyl acetate as a sole solvent in highly concentrated electrolyte for Li-ion batteries," *Electrochimica Acta*, vol. 154, pp. 287–293, 2015.

[76] D. W. McOwen, D. M. Seo, O. Borodin, J. Vatamanu, P. D. Boyle, and W. A. Henderson, "Concentrated electrolytes: Decrypting electrolyte properties and reassessing al corrosion mechanisms," *Energy & Environmental Science*, vol. 7, no. 1, pp. 416–426, 2014.

[77] Y. Yamada, Y. Takazawa, K. Miyazaki, and T. Abe, "Electrochemical lithium intercalation into graphite in dimethyl sulfoxide-based electrolytes: Effect of solvation structure of lithium ion," *The Journal of Physical Chemistry C*, vol. 114, no. 26, pp. 11 680–11 685, 2010.

[78] M. A. Gebbie, A. M. Smith, H. A. Dobbs, G. G. Warr, X. Banquy, M. Valtiner, M. W. Rutland, J. N. Israelachvili, S. Perkin, R. Atkin, *et al.*, "Long range electrostatic forces in ionic liquids," *Chemical Communications*, vol. 53, no. 7, pp. 1214–1224, 2017.

[79] D. R. MacFarlane, A. L. Chong, M. Forsyth, M. Kar, R. Vijayaraghavan, A. Somers, and J. M. Pringle, "New dimensions in salt–solvent mixtures: A 4th evolution of ionic liquids," *Faraday Discussions*, vol. 206, pp. 9–28, 2018.

[80] V. Nilsson, D. Bernin, D. Brandell, K. Edström, and P. Johansson, "Interactions and Transport in Highly Concentrated LiTFSI-based Electrolytes," *ChemPhysChem*, vol. 21, no. 11, pp. 1166–1176, 2020.

[81] D. M. Seo, O. Borodin, D. Balogh, M. O'Connell, Q. Ly, S.-D. Han, S. Passerini, and W. A. Henderson, "Electrolyte solvation and ionic association iii. acetonitrile-lithium salt mixtures–transport properties," *Journal of The Electrochemical Society*, vol. 160, no. 8, A1061, 2013.

[82] K. Dokko, D. Watanabe, Y. Ugata, M. L. Thomas, S. Tsuzuki, W. Shinoda, K. Hashimoto, K. Ueno, Y. Umebayashi, and M. Watanabe, "Direct evidence for Li-ion hopping conduction in highly concentrated sulfolane-based liquid electrolytes," *The Journal of Physical Chemistry B*, vol. 122, no. 47, pp. 10 736–10 745, 2018.

[83] X. Cao, H. Jia, W. Xu, and J.-G. Zhang, "Localized high-concentration electrolytes for lithium batteries," *Journal of The Electrochemical Society*, vol. 168, no. 1, p. 010 522, 2021.

[84] J. Qian, W. A. Henderson, W. Xu, P. Bhattacharya, M. Engelhard, O. Borodin, and J.-G. Zhang, "High rate and stable cycling of lithium metal anode," *Nature Communications*, vol. 6, no. 1, pp. 1–9, 2015.

[85] X. Fan, X. Ji, F. Han, J. Yue, J. Chen, L. Chen, T. Deng, J. Jiang, and C. Wang, "Fluorinated solid electrolyte interphase enables highly reversible solid-state Limetal battery," *Science Advances*, vol. 4, no. 12, eaau9245, 2018.

[86] J. Chen, Q. Li, T. P. Pollard, X. Fan, O. Borodin, and C. Wang, "Electrolyte design for Li metal-free Li batteries," *Materials Today*, vol. 39, pp. 118–126, 2020.

[87] Y. Zheng, F. A. Soto, V. Ponce, J. M. Seminario, X. Cao, J.-G. Zhang, and P. B. Balbuena, "Localized high concentration electrolyte behavior near a lithium–metal anode surface," *Journal of Materials Chemistry A*, vol. 7, no. 43, pp. 25 047–25 055, 2019.

[88] Y. Zheng, F. A. Soto, V. Ponce, J. Seminario, X. Cao, J.-G. Zhang, and P. Balbuena, "Localized high concentration electrolyte behavior near a lithium–metal anode surface," *Journal of Materials Chemistry A*, vol. 7, no. 43, pp. 25 047–25 055, 2019.

[89] X. Cao, X. Ren, L. Zou, M. H. Engelhard, W. Huang, H. Wang, B. E. Matthews, H. Lee, C. Niu, B. W. Arey, *et al.*, "Monolithic solid–electrolyte interphases formed in fluorinated orthoformate-based electrolytes minimize Li depletion and pulverization," *Nature Energy*, vol. 4, no. 9, pp. 796–805, 2019.

[90] J.-F. Ding, R. Xu, N. Yao, X. Chen, Y. Xiao, Y.-X. Yao, C. Yan, J. Xie, and J.-Q. Huang, "Non-solvating and low-dielectricity cosolvent for anion-derived solid electrolyte interphases in lithium metal batteries," *Angewandte Chemie International Edition*, vol. 60, no. 20, pp. 11 442–11 447, 2021.

[91] H. Lu, Y. Yuan, Z. Hou, Y. Lai, K. Zhang, and Y. Liu, "Solvate ionic liquid electrolyte with 1, 1, 2, 2-tetrafluoroethyl 2, 2, 2-trifluoroethyl ether as a support solvent for advanced lithium–sulfur batteries," *RSC Advances*, vol. 6, no. 22, pp. 18 186–18 190, 2016.

[92] A. Bouibes, S. Saha, and M. Nagaoka, "Theoretically predicting the feasibility of highly-fluorinated ethers as promising diluents for non-flammable concentrated electrolytes," *Scientific Reports*, vol. 10, no. 1, pp. 1–10, 2020.

[93] H. Lundgren, J. Scheers, M. Behm, and G. Lindbergh, "Characterization of the mass-transport phenomena in a superconcentrated LiTFSI: Acetonitrile electrolyte," *Journal of The Electrochemical Society*, vol. 162, no. 7, A1334, 2015.

[94] S. A. Krachkovskiy, J. D. Bazak, S. Fraser, I. C. Halalay, and G. R. Goward, "Determination of mass transfer parameters and ionic association of $LiPF_6$: Organic carbonates solutions," *Journal of The Electrochemical Society*, vol. 164, no. 4, A912, 2017.

[95] S. Krachkovskiy, M. Dontigny, S. Rochon, C. Kim, M. L. Trudeau, and K. Zaghib, "Determination of Binary Diffusivities in Concentrated Lithium Battery Electrolytes via NMR and Conductivity Measurements," *The Journal of Physical Chemistry C*, vol. 124, no. 45, pp. 24 624–24 630, 2020.

[96] S. Uchida and T. Kiyobayashi, "How does the solvent composition influence the transport properties of electrolyte solutions? LiPF6 and LiFSA in EC and DMC binary solvent," *Physical Chemistry Chemical Physics*, vol. 23, no. 18, pp. 10 875–10 887, 2021.

[97] M. Forsyth, H. Yoon, F. Chen, H. Zhu, D. R. MacFarlane, M. Armand, and P. C. Howlett, "Novel Na^+ Ion Diffusion Mechanism in Mixed Organic–Inorganic Ionic Liquid Electrolyte Leading to High Na^+ Transference Number and Stable, High Rate Electrochemical Cycling of Sodium Cells.," *The Journal of Physical Chemistry C*, vol. 120, no. 8, pp. 4276–4286, 2016.

[98] N. Agmon, "The grotthuss mechanism," *Chemical Physics Letters*, vol. 244, no. 5-6, pp. 456–462, 1995.

[99] Y. Yamada and A. Yamada, "Superconcentrated electrolytes for lithium batteries," *Journal of The Electrochemical Society*, vol. 162, no. 14, A2406, 2015.

[100] Y. Watanabe, Y. Ugata, K. Ueno, M. Watanabe, and K. Dokko, "Does li-ion transport occur rapidly in localized high-concentration electrolytes?" *Physical Chemistry Chemical Physics*, vol. 25, no. 4, pp. 3092–3099, 2023.

[101] S. P. Beltran, X. Cao, J.-G. Zhang, P. Z. El-Khoury, and P. B. Balbuena, "Influence of diluent concentration in localized high concentration electrolytes: elucidation of hidden diluent-Li^+ interactions and Li^+ transport mechanism," *Journal of Materials Chemistry A*, vol. 9, no. 32, pp. 17 459–17 473, 2021.

[102] Y. Wu, A. Wang, Q. Hu, H. Liang, H. Xu, and X. Wang Liand He, "Significance of antisolvents on solvation structures enhancing interfacial chemistry in localized high-concentration electrolytes," *ACS Central Science*, vol. 8, no. 9, pp. 1290–1298, 2022.

[103] M. Lacey, *Transport and transference in battery electrolytes*, http://lacey.se/science/transference/, 2023-03-04.

[104] O. Borodin, J. Self, K. A. Persson, C. Wang, and K. Xu, "Uncharted waters: Super-concentrated electrolytes," *Joule*, vol. 4, no. 1, pp. 69–100, 2020.

[105] N. P. Balsara and J. Newman, "Relationship between steady-state current in symmetric cells and transference number of electrolytes comprising univalent and multivalent ions," *Journal of The Electrochemical Society*, vol. 162, no. 14, A2720, 2015.

[106] J. Scheers, L. Niedzicki, G. Z. Żukowska, P. Johansson, W. Wieczorek, and P. Jacobsson, "Ion–ion and ion–solvent interactions in lithium imidazolide electrolytes studied by Raman spectroscopy and DFT models," *Physical Chemistry Chemical Physics*, vol. 13, no. 23, pp. 11 136–11 147, 2011.

[107] E. Flores, P. Novák, U. Aschauer, and E. J. Berg, "Cation Ordering and Redox Chemistry of Layered Ni-Rich Lix Ni1–2 y Co y Mn y O2: An Operando Raman Spectroscopy Study," *Chemistry of Materials*, vol. 32, no. 1, pp. 186–194, 2019.

[108] P. Jankowski, W. Wieczorek, and P. Johansson, "SEI-forming electrolyte additives for lithium-ion batteries: development and benchmarking of computational approaches," *Journal of Molecular Modeling*, vol. 23, pp. 1–9, 2017.

[109] K. Xu, "Nonaqueous liquid electrolytes for lithium-based rechargeable batteries," *Chemical reviews*, vol. 104, no. 10, pp. 4303–4418, 2004.

[110] X. Kang, "Electrolytes and interphases in Li-ion batteries and beyond," *Chemical reviews*, vol. 114, no. 23, pp. 11 503–11 618, 2014.

[111] D. M. Seo, O. Borodin, S.-D. Han, P. D. Boyle, and W. A. Henderson, "Electrolyte solvation and ionic association ii. acetonitrile-lithium salt mixtures: Highly dissociated salts," *Journal of The Electrochemical Society*, vol. 159, no. 9, A1489, 2012.

[112] D. Brouillette, D. E. Irish, N. J. Taylor, G. Perron, M. Odziemkowski, and J. E. Desnoyers, "Stable solvates in solution of lithium bis (trifluoromethylsulfone) imide in glymes and other aprotic solvents: Phase diagrams, crystallography and Raman spectroscopy," *Physical Chemistry Chemical Physics*, vol. 4, no. 24, pp. 6063–6071, 2002.

[113] Q. Wang, C. Zhao, J. Wang, Z. Yao, S. Wang, S. G. H. Kumar, S. Ganapathy, S. Eustace, X. Bai, B. Li, *et al.*, "High entropy liquid electrolytes for lithium batteries," *Nature Communications*, vol. 14, no. 1, p. 440, 2023.

[114] C. Yang, J. Xia, C. Cui, T. P. Pollard, J. Vatamanu, A. Faraone, J. A. Dura, M. Tyagi, A. Kattan, E. Thimsen, *et al.*, "All-temperature zinc batteries with high-entropy aqueous electrolyte," *Nature Sustainability*, pp. 1–11, 2023.

[115] M. Hellström and J. Behler, "Concentration-dependent proton transfer mechanisms in aqueous NaOH solutions: From acceptor-driven to donor-driven and back," *The Journal of Physical Chemistry Letters*, vol. 7, no. 17, pp. 3302–3306, 2016.

[116] R. A. Fisher, "Design of experiments," *British Medical Journal*, vol. 1, no. 3923, p. 554, 1936.

[117] L. Eriksson, E. Johansson, N. Kettaneh-Wold, C. Wikström, and S. Wold, "Design of experiments," *Principles and Applications, Learn ways AB, Stockholm*, 2000.